JCB Journal of Cell Biology

ARTICLE

VE-PTP stabilizes VE-cadherin junctions and the endothelial barrier via a phosphatase-independent mechanism

Vanessa V. Juettner[1], Kevin Kruse[1], Arkaprava Dan[2], Vinh H. Vu[2], Yousaf Khan[1], Jonathan Le[1], Deborah Leckband[2], Yulia Komarova[1], and Asrar B. Malik[1]

Vascular endothelial (VE) protein tyrosine phosphatase (PTP) is an endothelial-specific phosphatase that stabilizes VE-cadherin junctions. Although studies have focused on the role of VE-PTP in dephosphorylating VE-cadherin in the activated endothelium, little is known of VE-PTP's role in the quiescent endothelial monolayer. Here, we used the photoconvertible fluorescent protein VE-cadherin-Dendra2 to monitor VE-cadherin dynamics at adherens junctions (AJs) in confluent endothelial monolayers. We discovered that VE-PTP stabilizes VE-cadherin junctions by reducing the rate of VE-cadherin internalization independently of its phosphatase activity. VE-PTP serves as an adaptor protein that through binding and inhibiting the RhoGEF GEF-H1 modulates RhoA activity and tension across VE-cadherin junctions. Overexpression of the VE-PTP cytosolic domain mutant interacting with GEF-H1 in VE-PTP–depleted endothelial cells reduced GEF-H1 activity and restored VE-cadherin dynamics at AJs. Thus, VE-PTP stabilizes VE-cadherin junctions and restricts endothelial permeability by inhibiting GEF-H1, thereby limiting RhoA signaling at AJs and reducing the VE-cadherin internalization rate.

Introduction

Blood vessels are lined with an endothelial cell (EC) monolayer that forms a semipermeable barrier between the blood and surrounding interstitium (Pappenheimer et al., 1951; Del Vecchio et al., 1987). ECs in the continuous endothelium are connected by interendothelial junctions responsible for regulating transendothelial protein flux and leukocyte trafficking (Siflinger-Birnboim et al., 1987; Fujita et al., 1991; Feng et al., 1998). The interendothelial junctions thereby contribute to maintaining tissue-fluid homeostasis and innate immunity (Broermann et al., 2011; Vestweber, 2012; Zhao et al., 2017; Yeh et al., 2018). Disruption of these junctions leads to increased endothelial permeability as seen in inflammatory states, resulting in increased flux of plasma protein into tissue, edema formation, and trafficking of inflammatory cells (Mamdouh et al., 2009; Lee and Slutsky, 2010; Broermann et al., 2011).

Adherens junctions (AJs) and tight junctions (TJs) are multiprotein complexes formed between ECs responsible for regulating the paracellular permeability pathway (Corada et al., 2002; Heupel et al., 2009; Yuan and Rigor, 2010; Schulte et al., 2011). TJs in most vascular beds (except the brain and retina) are less developed than AJs and are not the primary determinants of endothelial barrier function (Komarova et al., 2017). AJs are composed of the adhesive protein vascular endothelial (VE)–cadherin, which forms a complex with catenin proteins, p120 catenin, and β-catenin (Breviario et al., 1995; Lampugnani et al., 1995; Navarro et al., 1995). VE-cadherin adhesion is regulated by phosphorylation and dephosphorylation on tyrosine residues (Lampugnani et al., 1997; Esser et al., 1998; Nawroth et al., 2002). Phosphorylation of VE-cadherin tyrosine residues 658, 685, and 731 causes dissociation of p120-catenin and β-catenin from VE-cadherin, leading to increased VE-cadherin internalization and weakening of the endothelial barrier (Baumeister et al., 2005; Potter et al., 2005; Xiao et al., 2005; Chiasson et al., 2009).

VE–protein tyrosine phosphatase (PTP) is a key EC-specific tyrosine phosphatase binding VE-cadherin through its membrane proximal fibronectin-like domain (FLD) at aa 1,449–1,619 (Nawroth et al., 2002). VE-PTP stabilizes endothelial barrier by supporting homotypic VE-cadherin adhesion that contributes to keeping basal endothelial permeability low (Nottebaum et al., 2008; Broermann et al., 2011; Vockel and Vestweber, 2013; Wessel et al., 2014). Knockdown of VE-PTP increases endothelial permeability and leukocyte extravasation (Nottebaum et al.,

[1]Department of Pharmacology and the Center for Lung and Vascular Biology, The University of Illinois College of Medicine, Chicago, IL; [2]Department of Chemical and Biomolecular Engineering, University of Illinois College of Engineering at Urbana-Champaign, Urbana, IL.

Correspondence to Asrar B. Malik: abmalik@uic.edu; Yulia A. Komarova: ykomarov@uic.edu.

2008), whereas preventing VE-PTP and VE-cadherin dissociation inhibits these events (Broermann et al., 2011). VE-PTP also counterbalances the effects of permeability-increasing mediators such as VEGF, which increase endothelial permeability and leukocyte trafficking, by dephosphorylating VE-cadherin at Tyr658 and Tyr685, leading to stabilization of VE-cadherin junctions (Wallez et al., 2007; Nottebaum et al., 2008; Orsenigo et al., 2012).

While studies have focused on the relationship of VE-PTP and VE-cadherin in activated ECs (Nottebaum et al., 2008; Broermann et al., 2011; Vockel and Vestweber, 2013), little is known about the role of VE-PTP in the resting endothelial barrier. Although VE-PTP depletion in the endothelium increases endothelial permeability, it has minimal effect on VE-cadherin phosphorylation (Nottebaum et al., 2008). We therefore addressed the possibility that VE-PTP regulates basal endothelial permeability independently of its enzymatic activity. Here, we report a novel adaptor function of VE-PTP required to stabilize VE-cadherin junctions and restrict basal endothelial permeability.

Results

VE-PTP reduces VE-cadherin internalization in the quiescent endothelium

We observed increased endothelial permeability (Fig. 1, A and B) in response to siRNA-mediated knockdown of VE-PTP in ECs (Fig. S1, A and B), consistent with VE-PTP's known key role in stabilizing VE-cadherin junctions and restricting basal endothelial permeability (Nottebaum et al., 2008). Since the rate of VE-cadherin internalization regulates junctional permeability (Gavard and Gutkind, 2006; Hou et al., 2011; Vandenbroucke St Amant et al., 2012; Gong et al., 2014), we addressed the role of VE-PTP in regulating VE-cadherin dynamics in quiescent endothelial monolayers. Here, we used the irreversible, photoconvertible fluorescent protein Dendra2 attached to the C terminus of VE-cadherin (VE-cad-Dendra2; Chudakov et al., 2007; Daneshjou et al., 2015). We monitored VE-cadherin dynamics after irradiating the expressed Dendra2 using a laser to induce an emission shift from 488 nm to 543 nm, specifically within the irradiation zone (Chudakov et al., 2007). We observed that VE-PTP depletion increased VE-cadherin internalization rate as compared with cells treated with non-targeting (NT) siRNA (Fig. 1, C–E). Importantly, this occurred without a change in the VE-cadherin recruitment rate to AJs (Fig. S1 C). Along with the faster VE-cadherin internalization rate and increased permeability in VE-PTP–deleted cells, we also observed reduced VE-cadherin junctional area (Fig. S1, D and E). VE-cadherin protein expression, however, did not change (Fig. S1, F and G). Thus, these results showed that VE-PTP modulates the VE-cadherin internalization rate in the quiescent endothelium and thereby stabilizes VE-cadherin junctions and reduces endothelial permeability.

The VE-PTP extracellular domain consists of 17 FLDs, of which the most plasmalemmal proximal, the 17th FLD, interacts with VE-cadherin extracellular domain 5 (Nawroth et al., 2002). We used deletion mutants lacking 16 (Δ16FN) or all FLDs (ΔN) in addition to full-length (WT) VE-PTP (Figs. 1 F and S1 H) to identify the VE-PTP extracellular domain regulating VE-cadherin internalization. Overexpression of WT or Δ16FN VE-PTP markedly reduced the VE-cadherin internalization rate as compared with overexpressing control fluorescent tag alone (Fig. 1, G–I), whereas overexpression of ΔN mutant, which accumulated poorly at AJs, had no effect on VE-cadherin dynamics (Fig. 1, G–I). Overexpression of WT VE-PTP also had no effect on the VE-cadherin recruitment rate (Fig. S1 C). These data thus demonstrated that the 17th FLD interacting with VE-cadherin was essential for stabilizing AJs by preventing VE-cadherin internalization.

As VE-PTP is known to promote the adhesion of CHO cells to VE-cadherin–coated surfaces (Nawroth et al., 2002), we addressed the possibility that VE-PTP regulates the binding affinity of VE-cadherin trans-interaction and thereby controls VE-cadherin junction stability. Studies were made using the dual micropipette system in which VE-cadherin trans-interactions were measured between RBCs expressing the human VE-cadherin-Fc fragment and mouse lung endothelial cells (MLECs) isolated from either *VE-PTP*$^{flox/flox}$ (WT) or *VE-PTP*$^{-/-}$ (knockout [KO]) mice (Quaggin, 2017; Souma et al., 2018; Fig. S1 I). VE-PTP KO had no significant effect on the binding affinity (k_A) or off-rate (k_{off}) of VE-cadherin trans-interactions (Fig. S1, J and K). Thus, although interaction between VE-PTP and VE-cadherin was required for stabilizing AJs, VE-PTP did not allosterically regulate VE-cadherin trans-interactions, ruling out this mechanism in mediating the stability of AJs.

VE-PTP mediates the stability of VE-cadherin junctions independently of phosphatase activity

Because studies have demonstrated that VE-PTP knockdown or inhibition of phosphatase activity did not induce VE-cadherin phosphorylation in resting endothelial monolayers (Nottebaum et al., 2008; Gurnik et al., 2016), we determined whether the VE-PTP phosphatase activity per se is required for VE-PTP–dependent stabilization of VE-cadherin junctions. Thus, we used a VE-PTP phosphatase inactive (PI) mutant containing a D/A (aspartic acid to alanine) point mutation at a 1,871 (Fig. 2 A). We observed that VE-PTP PI overexpression reduced the VE-cadherin internalization rate to levels seen in WT VE-PTP–expressing cells (Fig. 2, B–D), indicating that VE-PTP catalytic activity in the quiescent endothelium did not regulate VE-PTP–dependent VE-cadherin internalization. Similarly, the VE-PTP phosphatase inhibitor AKB-9785 (Shen et al., 2014; Gurnik et al., 2016) had no effect on either VE-cadherin phosphorylation or internalization rates (Fig. S2, A–H) consistent with VE-PTP–mediated stabilization of VE-cadherin junctions occurring independently of VE-PTP phosphatase activity. To determine whether the cytosolic domain of VE-PTP was required for stabilizing VE-cadherin, we overexpressed a VE-PTP deletion mutant lacking the cytosolic domain (ΔC; Fig. 2 A and Fig. S1 H). We observed that overexpression of ΔC VE-PTP mutant, in contrast to full-length VE-PTP, did not reduce the VE-cadherin internalization rate (Fig. 2, B–D). These studies thus showed that the cytosolic domain of VE-PTP functioning independently of phosphatase activity was essential for VE-cadherin junction stabilization.

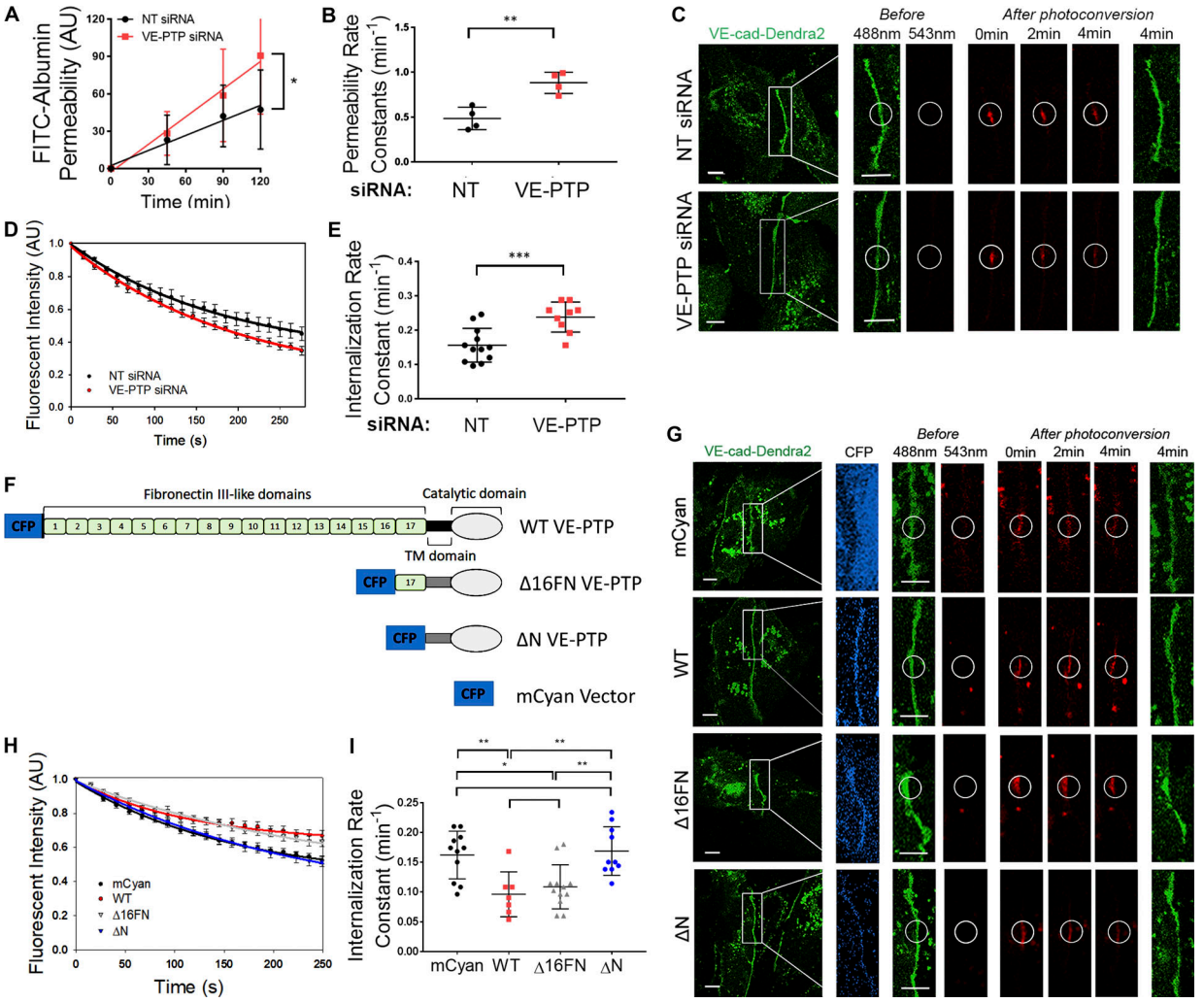

Figure 1. **VE-PTP stabilizes the endothelial barrier by decreasing the VE-cadherin internalization rate. (A)** Permeability of HPAEC monolayers to FITC-conjugated albumin tracer after treatment with NT (control) siRNA or VE-PTP siRNA; mean ± SEM, *n* = 3–4 independent experiments; *, P < 0.05, unpaired *t* test. **(B)** Endothelial permeability rate constants of 0.48 ± 0.06 min^{-1} and 0.88 ± 0.05 min^{-1} in cells from A treated with NT siRNA or VE-PTP siRNA, respectively; mean ± SEM; *n* = 3–4; **, P < 0.001, unpaired *t* test. **(C)** Time-lapse images of VE-cad-Dendra2 emitting green fluorescence before photoconversion and red fluorescence after photoconversion within a selected region (indicated by circle) in HPAECs treated with NT siRNA or VE-PTP siRNA. Scale bars, 5 µm. **(D)** VE-cadherin internalization rate (decay in red fluorescence within photoconversion zone in C) in NT siRNA and VE-PTP siRNA-treated HPAECs; mean ± SEM; *n* = 9–12 junctions from four independent experiments. **(E)** Internalization rate constants of 0.15 ± 0.01 min^{-1} and 0.23 ± 0.01 min^{-1} from data in D in cells treated with NT siRNA or VE-PTP siRNA, respectively; mean ± SEM; *n* = 9–12 junctions from four independent experiments; ***, P < 0.0001, unpaired *t* test. **(F)** Schematic representation of VE-PTP mutants used in G–I; mCyan (control), full-length (WT) VE-PTP, Δ16FN VE-PTP mutant (lacking FN1-16 but capable of binding to VE-cadherin via intact 17th FN domain), or ΔN VE-PTP mutant (lacking entire extracellular VE-PTP domain). **(G)** Time-lapse images of VE-cad-Dendra2 in HPAECs overexpressing constructs in F. Scale bar, 5 µm. **(H)** VE-cadherin internalization rates from AJs in HPAECs transfected with constructs in F; mean ± SEM; *n* = 7–12 junctions from four independent experiments. **(I)** Internalization rate constants from data in H in cells overexpressing mCyan (0.16 ± 0.012 min^{-1}), WT VE-PTP (0.09 ± 0.01 min^{-1}), Δ16FN (0.10 ± 0.01 min^{-1}), or ΔN (0.16 ± 0.01 min^{-1}); mean ± SEM; *n* = 7–12 junctions from four independent experiments; *, P < 0.05; **, P < 0.001, one-way ANOVA.

The observed effects of VE-PTP mutants on VE-cadherin internalization corresponded to their effects on endothelial permeability (Fig. S2 I). Overexpression of VE-PTP mutants stabilizing VE-cadherin junctions also reduced endothelial permeability as compared with mCyan control (Fig. S2 I). Stabilization of VE-cadherin junctions occurred without any apparent changes in VE-cadherin phosphorylation (Fig. S2, J–L), reinforcing our findings that stabilization of VE-cadherin junctions did not require VE-PTP phosphatase activity.

VE-PTP interacts with GEF-H1

We next addressed the possibility that VE-PTP controls VE-cadherin internalization by regulating RhoGTPase signaling, an essential VE-cadherin junction–modulating pathway (Daneshjou et al., 2015). To identify the RhoGTPase signaling pathway regulated by VE-PTP, we performed mass spectrometry of the immunoprecipitated VE-PTP protein complex from EC lysates. We identified ARHGEF2 (also known as GEF-H1) as the primary RhoGTPase-binding VE-PTP (Fig. S3, A and B). Reverse immunoprecipitation studies in which GEF-H1 coprecipitated with

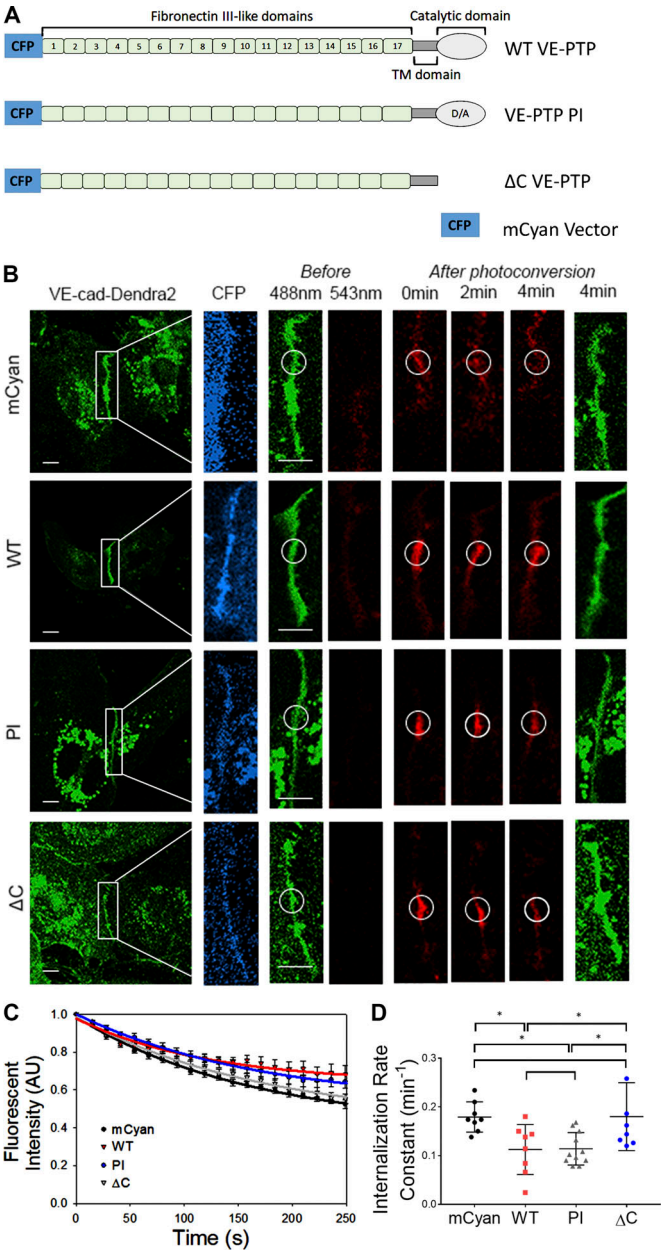

Figure 2. **VE-PTP phosphatase activity is not required for stabilization of VE-cadherin junctions in the quiescent endothelium. (A)** Schematic representation of VE-PTP mutants overexpressed in HPAECs; mCyan, WT VE-PTP, VE-PTP PI, and VE-PTP ΔC (lacking cytoplasmic domain) mutants. **(B)** Time-lapse images of VE-cad-Dendra2 in HPAECs overexpressing constructs in A. Scale bars, 5 µm. **(C)** VE-cadherin internalization from AJs in HPAECs overexpressing constructs in A; mean ± SEM; *n* = 8–11 junctions from three to four independent experiments. **(D)** Internalization rate constants calculated from C in cells overexpressing mCyan (0.17 ± 0.01 min^{-1}), WT (0.11 ± 0.01 min^{-1}), VE-PTP PI (0.11 ± 0.01 min^{-1}), and ΔC VE-PTP (0.18 ± 0.02 min^{-1}); mean ± SEM; *n* = 8–11 from three to four independent experiments; *, P < 0.05, one-way ANOVA.

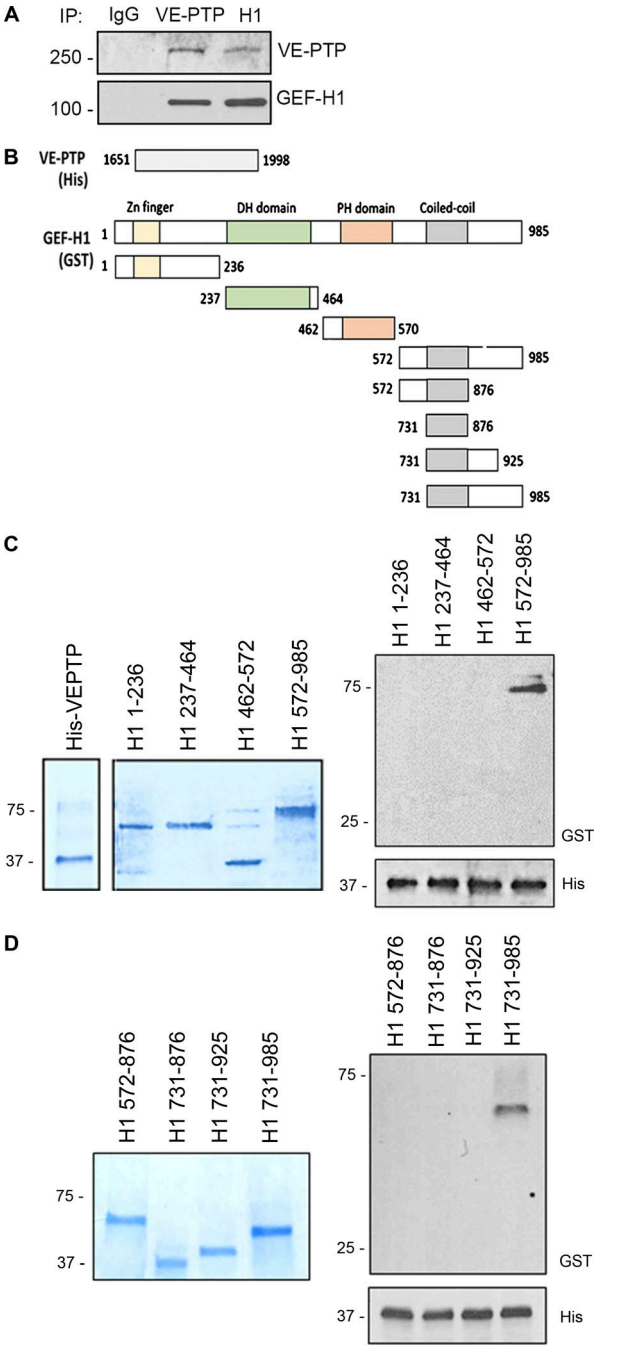

Figure 3. **VE-PTP interacts with C terminus of GEF-H1. (A)** Reverse immunoprecipitation (IP) of endogenous VE-PTP or GEF-H1 proteins from HPAEC lysates. Blots were probed for GEF-H1 and VE-PTP. **(B)** Schematic representation of indicated His-tagged C terminus of VE-PTP and GST-tagged GEF-H1 deletion mutants. **(C and D)** Domain interaction of GEF-H1 tested in pull-down experiments. Gel electrophoresis stained with Coomassie blue of bacteria purified proteins indicated in B (left). Direct interactions between cytosolic domain of His-VE-PTP (aa 1,651–1,998) and various GEF-H1 deletion mutants (right) detected by Western blot analysis.

VE-PTP and vice versa confirmed this interaction (Fig. 3 A). To determine GEF-H1 domains interacting with VE-PTP, we performed binding experiments using bacteria purified GST-tagged GEF-H1 deletion mutants and cytosolic domain of His-tagged VE-PTP (Fig. 3, B–D). The cytoplasmic domain of VE-PTP (aa 1,651–1,998) was shown to interact with the C-terminal domain of GEF-H1 (aa 572–985; Fig. 3 C). Further deletions of GEF-H1 C terminus showed that the most proximal domain (aa 925–985) was primarily responsible for VE-PTP interactions (Fig. 3 D).

VE-PTP inhibits GEF-H1 binding to RhoA and reduces RhoA activity at AJs

GEF-H1 is a guanine nucleotide exchange factor promoting the exchange of RhoA GDP to GTP and inducing RhoA activation (Ren et al., 1998; Krendel et al., 2002; Nalbant et al., 2009). We surmised that GEF-H1 binding to VE-PTP might regulate GEF activity and RhoA signaling at AJs to control VE-cadherin junction stability. Using nucleotide-free RhoA (G17A), the form of RhoA exhibiting the highest binding to active RhoGEFs, we determined the amount of nucleotide-free RhoA-bound GEF-H1 in ECs treated with control siRNA, GEF-H1 siRNA, or VE-PTP siRNA. VE-PTP depletion markedly increased GEF-H1 binding to nucleotide-free RhoA, indicating increased GEF-H1 activity, whereas GEF-H1 depletion reduced GEF-H1 activity as compared with control cells (Fig. 4, A and B). Furthermore, GEF-H1 tyrosine phosphorylation was undetectable in cells treated with either control or VE-PTP siRNA (data not shown), indicating that VE-PTP did not function by dephosphorylating GEF-H1. Thus, the interaction between VE-PTP and GEF-H1 reduced GEF-H1 binding to RhoA and thereby blocked GEF-H1 function.

Depletion of VE-PTP also significantly decreased GEF-H1 accumulation at AJs (Fig. 4, C and D) that occurred without a change in GEF-H1 protein expression (Fig. S3, C and D). We also observed that overexpressing WT VE-PTP restored GEF-H1 accumulation at AJs in VE-PTP–depleted endothelial monolayers (Fig. S3, E and F), but this was not seen in ECs overexpressing the VE-PTP ΔC mutant lacking the GEF-H1 interacting domain (Fig. S3, E and F). Thus, the VE-PTP's cytosolic domain was essential for VE-PTP–dependent accumulation of GEF-H1 at AJs.

Since GEF-H1 can also be inhibited through binding to the TJ protein cingulin and microtubules (Ren et al., 1998; Aijaz et al., 2005; Tsai et al., 2008; Schossleitner et al., 2016), we addressed the possibility that depletion of VE-PTP could influence intracellular distribution of cingulin or cause reorganization of the microtubule cytoskeleton. However, depletion of VE-PTP had no effect on the expression or distribution of cingulin in ECs (Fig. S3, G–J), suggesting that cingulin was not responsible for inhibiting GEF-H1. Depletion of VE-PTP, however, reorganized cortical F-actin into stress fibers accompanied by reduced F-actin area (Fig. S3, K and L). Loss of cortical actin was likely a result of destabilization of VE-cadherin junctions (Komarova et al., 2012). VE-PTP depletion was also accompanied by reorganization of microtubules, which became aligned with F-actin fibers (Fig. S3 K); however, this occurred without a change in the microtubule area (Fig. S3 M), suggesting that reorganization of the microtubule cytoskeleton is unlikely to be responsible for GEF-H1 activation in VE-PTP–depleted cells.

We next investigated the role of VE-PTP in regulating RhoA and Rac1 activities at AJs using Förster resonance energy transfer (FRET)–based biosensors for RhoA (Pertz et al., 2006) and Rac1 (MacNevin et al., 2016). Knockdown of VE-PTP increased RhoA activity at AJs without altering cytosolic RhoA activity (Fig. 4, E–G). This change in RhoA activity seen in VE-PTP–depleted cells was not accompanied by a change in Rac1 activity (Fig. S4, A and B), showing that VE-PTP is solely responsible for RhoA signaling at AJs. Overexpression of WT VE-PTP and the C terminus domain of VE-PTP (aa 1,651–1,998), which both bind GEF-H1, in ECs depleted of VE-PTP significantly reduced RhoA activity at AJs (Fig. S4, C and D). However, the VE-PTP ΔC mutant lacking the GEF-H1 interacting domain failed to reduce RhoA activity at AJs (Fig. S4, C and D). Furthermore, knockdown of GEF-H1 decreased RhoA activity at AJs in both control and VE-PTP–depleted ECs (Fig. 4, E and F; and Fig. S4, E–I). Although some reduction in cytosolic RhoA activity was seen in GEF-H1–depleted cells, the change was not significant (Fig. 4 G). These results show that VE-PTP inhibits GEF-H1 activation and reduces RhoA signaling at the level of AJs in the quiescent endothelium.

We also observed that overexpression of WT VE-PTP reduced GEF-H1 binding to RhoA (Fig. 4, H and I) that was accompanied by reduced RhoA activity at AJs as compared with control ECs expressing fluorescent tag (Fig. 4, J and K). In addition, overexpression of VE-PTP PI mutant reduced RhoA activity at AJs (Fig. 4, J and K), consistent with the central observation that VE-PTP phosphatase activity did not regulate VE-cadherin dynamics at AJs (Fig. 2). Consistent with the proposed role of VE-PTP in modulating RhoA signaling, overexpression of the VE-PTP PI mutant had no effect on Rac1 activity at AJs (Fig. S4, J and K). Together, these data demonstrate that VE-PTP reduced RhoA activity at AJs without altering Rac1 activity and thereby stabilized VE-cadherin junctions.

VE-PTP relieves tension across VE-cadherin junctions

Since RhoA activation increases tension applied across VE-cadherin junctions (Daneshjou et al., 2015), we next addressed whether VE-PTP–dependent inhibition of GEF-H1 activity reduces actomyosin-mediated tension to enhance endothelial barrier function. To quantify tension changes at AJs, we used the VE-cadherin FRET-based tension biosensor (Conway et al., 2013). VE-PTP knockdown increased the tension applied at AJs as compared with endothelial monolayers treated with control siRNA (Fig. 5, A and B). Consistent with the role of VE-PTP in reducing GEF-H1 binding to RhoA, we observed that knockdown of GEF-H1 reduced tension across VE-cadherin junctions in both control and VE-PTP–depleted ECs (Fig. 5, A and B). Further, we observed that overexpression of WT VE-PTP or VE-PTP PI also reduced the tension applied to VE-cadherin in quiescent monolayers (Fig. 5, C and D), consistent with the inability of VE-PTP phosphatase activity in regulating RhoA activity at AJs (Fig. 4, H and I).

Interestingly, overexpression of WT VE-PTP, but not VE-PTP PI mutant, significantly reduced tension across VE-cadherin junctions in ECs challenged with α-thrombin (Fig. S4, L and M), known to activate RhoA signaling (van Nieuw Amerongen et al., 2000). Although WT and PI mutants were similarly expressed and accumulated at AJs (Fig. S4, N and O), overexpression of PI mutant did not reduce tension applied to AJs as in the case of WT VE-PTP in endothelial monolayers challenged with α-thrombin (Fig. S4, L and M). These data support the distinct functions of VE-PTP in the quiescent endothelium as opposed to endothelium activated with a proinflammatory stimulus, α-thrombin.

To validate the tension change measurements occurring at AJs by the biosensor described above, we also alternatively

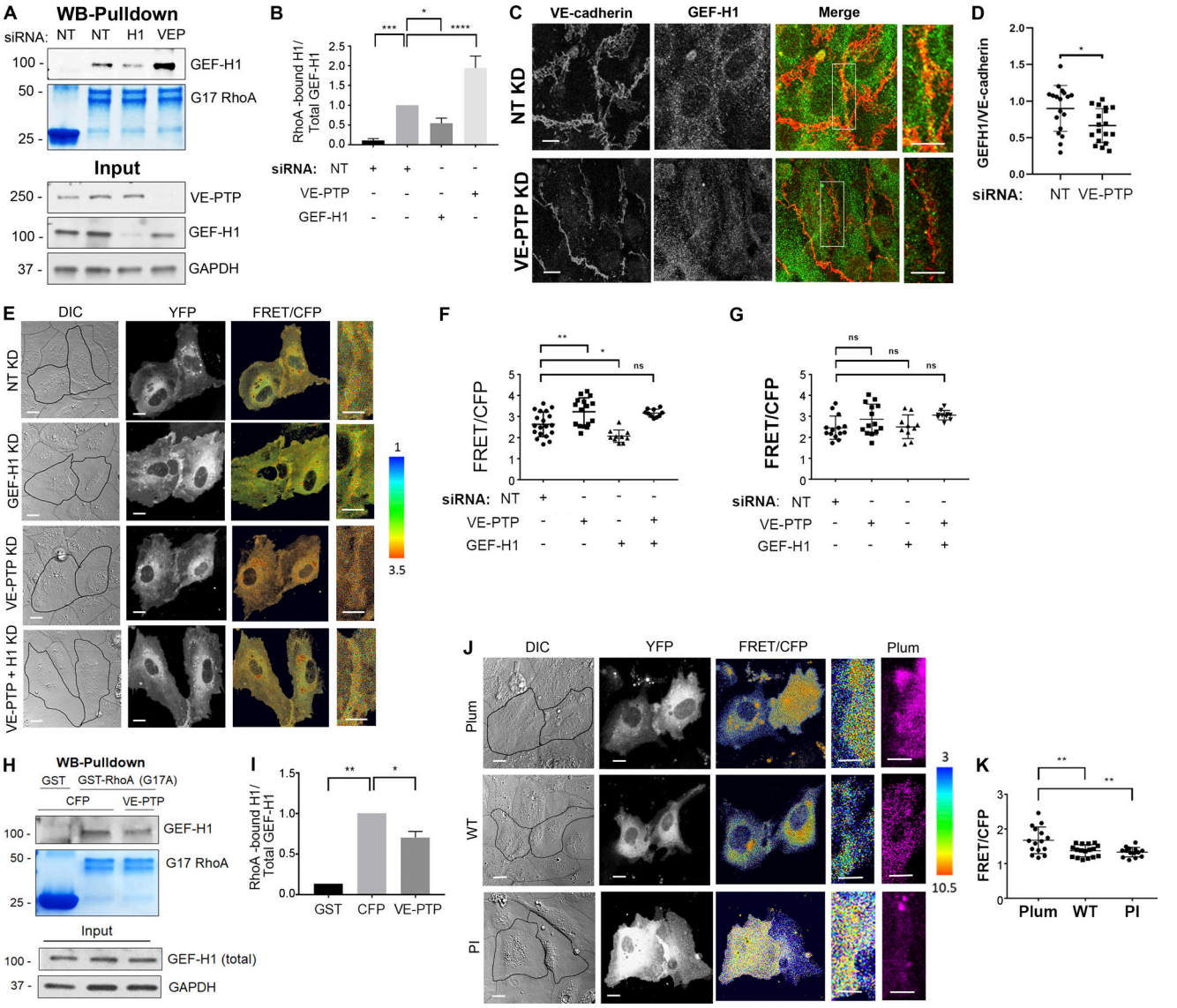

Figure 4. **VE-PTP reduces GEF-H1 binding to RhoA and inhibits RhoA activity at VE-cadherin junctions. (A and B)** Interaction of GEF-H1 with GST-RhoA (G17A) in HPAECs treated with NT siRNA or VE-PTP siRNA. The resulting precipitates were probed for GEF-H1 (A) and quantification of data (B); mean ± SEM; $n = 3$; *, $P < 0.05$; **, $P < 0.001$; ****, $P < 0.0001$; one-way ANOVA. **(C)** Immunofluorescent images of VE-cadherin (red) and GEF-H1 (green) in confluent HPAEC monolayers treated with NT siRNA or VE-PTP siRNA. Scale bars, 5 µm. **(D)** Analysis of GEF-H1 expression at VE-cadherin junctions from data in C; mean ± SEM, $n = 18$ images per group from two independent experiments. **(E)** Differential interference contrast (DIC) and confocal images of biosensor (YFP) and RhoA activity (FRET/CFP) in HPAECs treated with NT siRNA or siRNA against VE-PTP, GEF-H1, or both proteins. The ratiometric images were scaled from 1 to 3.5 and color-coded as indicated on right. Warmer colors denote higher RhoA activity. Scale bars, 5 µm. **(F and G)** Relative RhoA activity at the AJs (F) or in cytosol (G) of cells in E; mean ± SEM; $n = 10–19$ junctions from three independent experiments; *, $P < 0.05$; **, $P < 0.001$; one-way ANOVA. **(H and I)** Interaction of GEF-H1 with GST-RhoA (G17A) in HPAECs overexpressing CFP or CFP-VE-PTP. The resulting precipitates were probed for GEF-H1 using Western blot analysis (H) and quantification of data (I). GST precipitates from CFP-expressing cells used as a control; $n = 2$; *, $P < 0.05$; **, $P < 0.001$; one-way ANOVA. **(J)** DIC and confocal images of biosensor (YFP) and RhoA activity (FRET/CFP) in HPAECs expressing mPlum (control), mPlum-VE-PTP (WT), or mPlum-VE-PTP PI (PI). The ratiometric images were scaled from 3 to 10.5 and color-coded as indicated on the right. Scale bars, 5 µm. **(K)** Relative RhoA activity at AJs of cells shown in H; mean ± SEM; $n = 14–17$ junctions from three independent experiments; **, $P < 0.001$; one-way ANOVA. KD, knockdown.

determined the role of VE-PTP in modulating tension across AJs using the micropillar array assay (Yang et al., 2011). This measurement is similar to that obtained with the VE-cadherin biosensor described above (see Materials and methods), the primary difference being that it allows determination of the force applied to AJs in absolute units. We observed that *VE-PTP*$^{-/-}$ MLECs exhibited increased stress at AJs as compared with *VE-PTP*$^{flox/flox}$ (WT) MLECs (Fig. S4, P–S), confirming the results above with the VE-cadherin tension biosensor. Furthermore, analysis of traction forces using the bead displacement assay also demonstrated that VE-PTP deletion had no effect on tension development in single ECs (Fig. S4 T), consistent with the tension-reducing function of VE-PTP being confined only to VE-cadherin junctions as described above.

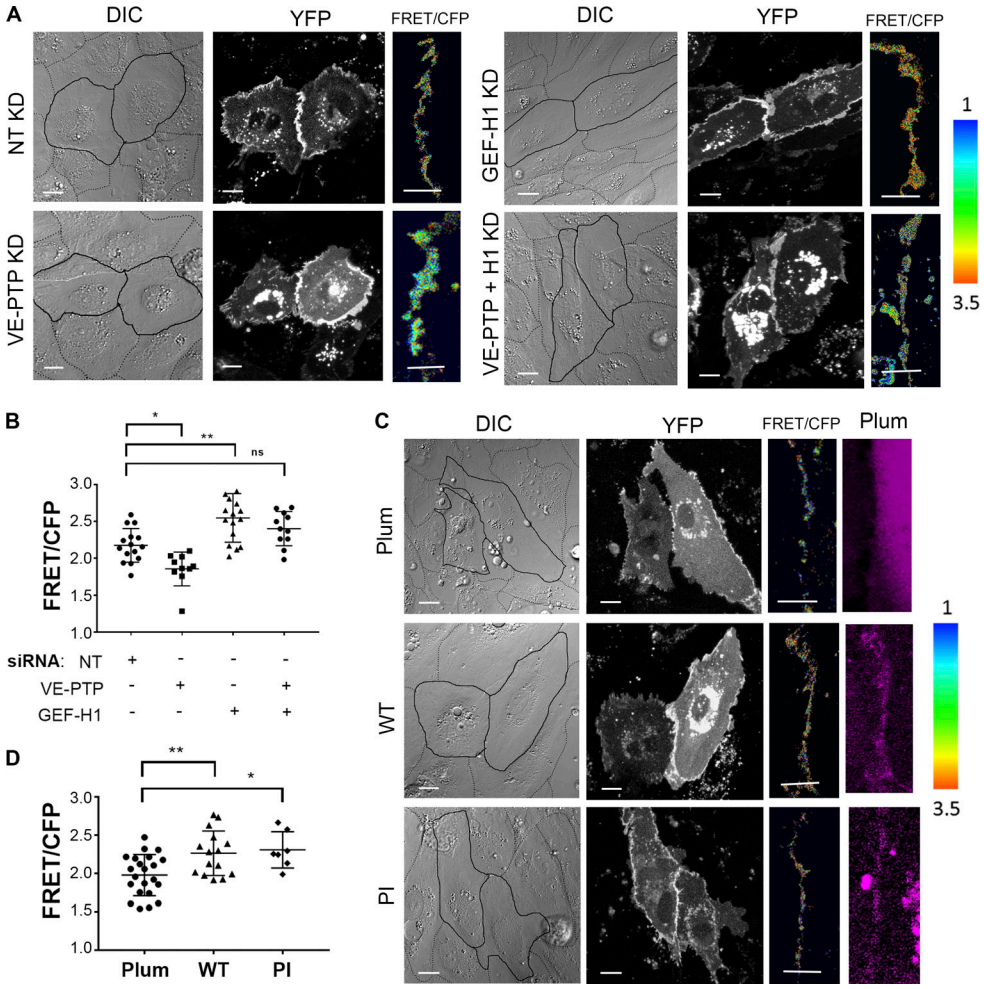

Figure 5. **VE-PTP relieves tension across VE-cadherin junctions in the quiescent endothelium. (A)** DIC and confocal images of VE-cadherin biosensor (YFP) and VE-cadherin tension (FRET/CFP) in HPAECs depleted of VE-PTP, GEF-H1, or both. The ratiometric images scaled from 1 to 3.5 and color coded as indicated on right. Warmer colors denote low tension. Scale bars, 5 µm. **(B)** Relative tension at AJs for groups in A. Higher values denote lower tension; mean ± SEM; *n* = 10–15 junctions from three independent experiments; *, P < 0.05; **, P < 0.001; one-way ANOVA. **(C)** DIC and confocal images of VE-cadherin biosensor (YFP) and VE-cadherin tension (FRET/CFP) in HPAECs overexpressing mPlum (control), mPlum-VE-PTP (WT), or mPlum-VE-PTP PI (PI). The ratiometric images are scaled as in A. Scale bars, 5 µm. **(D)** Relative tension at AJs for groups in C; mean ± SEM; *n* = 8–16 junctions from three independent experiments; *, P < 0.05; **, P < 0.001; one-way ANOVA. KD, knockdown.

GEF-H1 knockdown or overexpression of VE-PTP cytosolic domain restores VE-cadherin internalization rates in VE-PTP–deficient ECs

We next compared the role of GEF-H1 (ARHGEF2) in mediating stabilization of VE-cadherin junctions by measuring VE-cadherin internalization rates in endothelial monolayers depleted of GEF-H1 (Fig. 6, A–C) as well as monolayers depleted of other related RhoGEFs (Fig. S5, A–E). Knockdown of GEF-H1 significantly reduced the VE-cadherin internalization rate as compared with cells treated with control siRNA (Fig. 6, A–C). In contrast, knockdown of ARHGEF1 (p115RhoGEF), ARHGEF18 (p114RhoGEF), or ARHGEF28 (p190RhoGEF), also known to regulate RhoA activity (Gebbink et al., 1997; Hart et al., 1998; Kozasa et al., 1998; Holinstat et al., 2003; Niu et al., 2003; Abiko et al., 2015; Tornavaca et al., 2015), did not show reduced VE-cadherin internalization rates as compared with GEF-H1 (ARHGEF2; Fig. S5, A–E). Furthermore, GEF-H1 depletion reduced both the VE-cadherin internalization rate and permeability values in ECs depleted of VE-PTP (Fig. 6, A–E).

To investigate the role of VE-PTP interactions with GEF-H1 in regulating VE-cadherin dynamics at AJs, we determined the effects of overexpressing the VE-PTP cytosolic domain (C domain), which interacts with GEF-H1, in vitro (Fig. 3 D) and in endothelial monolayers (Fig. 7 A). We found that overexpression of the VE-PTP C domain significantly reduced GEF-H1 binding to RhoA in endothelial monolayers depleted of VE-PTP (Fig. 7, B and C). Furthermore, overexpression of the VE-PTP C domain reduced the VE-cadherin internalization rate and endothelial permeability to albumin in VE-PTP–depleted ECs (Fig. 7, D–H), indicating a causal link between VE-PTP and GEF-H1 in regulating both VE-cadherin junction stability and endothelial barrier permeability.

To establish the relationship between RhoA signaling and VE-cadherin dynamics at AJs, we also pharmacologically activated

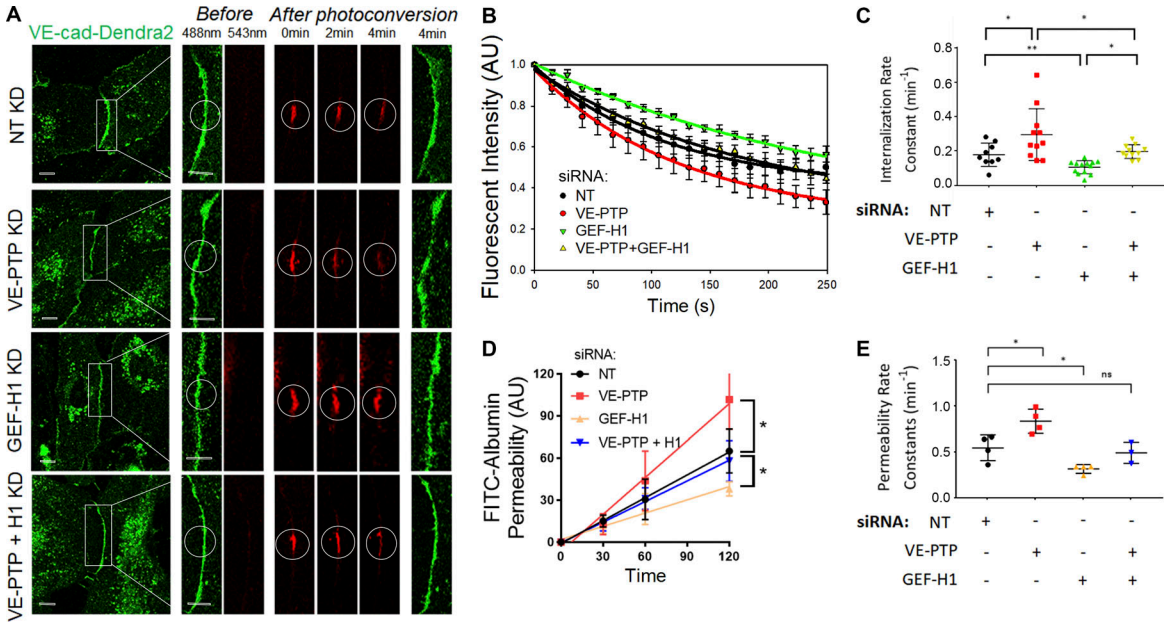

Figure 6. **GEF-H1 knockdown restores VE-cadherin internalization rate in VE-PTP–depleted endothelial monolayers. (A)** VE-cad-Dendra2 before (green) and after (red) photoconversion in HPAECs depleted of VE-PTP, GEF-H1, or VE-PTP and GEF-H1 simultaneously. Scale bars, 5 µm. **(B)** VE-cadherin internalization from AJs from data in A; mean ± SEM; *n* = 9–13 junctions from three independent experiments. **(C)** Internalization rate constants calculated from B were 0.17 ± 0.02 min^{-1} in NT siRNA–treated cells, 0.29 ± 0.04 min^{-1} and 0.10 ± 0.01 min^{-1} in VE-PTP– and GEF-H1–depleted cells, or 0.19 ± 0.01 min^{-1} after simultaneous depletion of VE-PTP and GEF-H1; mean ± SEM; *n* = 9–13 junctions from three independent experiments; *, P < 0.05; **, P < 0.001; one-way ANOVA. **(D)** Permeability of HPAEC monolayers to FITC-conjugated albumin in HPAECs depleted of VE-PTP, GEF-H1, or VE-PTP and GEF-H1 simultaneously; *n* = 3–4. *, P < 0.05; one-way ANOVA. **(E)** Permeability rate constants from D were 0.54 ± 0.06 min^{-1} in NT siRNA–treated cells, 0.83 ± 0.06 min^{-1} and 0.31 ± 0.02 min^{-1} after VE-PTP and GEF-H1 depletion, or 0.49 ± 0.06 min^{-1} after simultaneous depletion of VE-PTP and GEF-H1; mean ± SEM; *n* = 3–4; *, P < 0.05; one-way ANOVA. KD, knockdown.

Rho signaling or inhibited Rho-associated protein kinase (ROCK). Activation of Rho with CN-01 increased VE-cadherin internalization rate, whereas inhibition of ROCK with Rockout decreased VE-cadherin internalization rate in quiescent confluent monolayers (Fig. S5, F and G). These findings support the model in which VE-PTP stabilizes VE-cadherin junctions and reduces endothelial permeability by inhibiting GEF-H1, RhoA activity, and tension at junctions and thereby decreases the rate of VE-cadherin internalization.

Discussion

We demonstrate that VE-PTP, the receptor-like, transmembrane protein tyrosine phosphatase (Fachinger et al., 1999; Alonso et al., 2004), serves a scaffold function at AJs of ECs. VE-PTP binds and inhibits the guanine nucleotide exchange factor GEF-H1 (Ren et al., 1998; Krendel et al., 2002), and VE-PTP, through this mechanism, reduces the rate of VE-cadherin internalization. This scaffold function of VE-PTP requires its cytosolic domain, but not its phosphatase activity. In this regard, VE-PTP resembles PTP-PEST, a cytosolic member of the PTP family that also forms a protein complex independent of the protein's catalytic activity (Davidson and Veillette, 2001).

We identified GEF-H1 through high-throughput analysis of VE-PTP interacting partners. GEF-H1 promotes the exchange of RhoA GDP to GTP, leading to activation of RhoA (Ren et al., 1998; Krendel et al., 2002). We demonstrated that overexpression of full-length or the cytosolic portion of VE-PTP significantly reduced GEF-H1 binding to RhoA and consequently inhibited RhoA activity at endothelial AJs. Thus, the binding of VE-PTP to GEF-HI functions to inhibit GEF-H1 activity. In contrast, depletion of VE-PTP resulted in activation of RhoA specifically at AJs. These findings suggest that VE-PTP spatially inhibits RhoA activity at AJs, similar to the role of the TJ protein cingulin in epithelial cells that also prevents RhoA activity at TJs through interaction with GEF-H1 (Aijaz et al., 2005).

The mechanism of VE-PTP modulation of GEF-H1 activity is unknown. GEF-H1 activity may be regulated by protein–protein interaction (Ren et al., 1998; Krendel et al., 2002; Aijaz et al., 2005) and GEF-H1 phosphorylation at serine and threonine residues (Zenke et al., 2004; Birkenfeld et al., 2007; Fujishiro et al., 2008; von Thun et al., 2013). However, we found that VE-PTP did not dephosphorylate GEF-H1 at tyrosine residues, ruling out this mechanism. A more tenable possibility is that GEF-H1 binding to VE-PTP stabilizes GEF-H1 in an inactive conformation and prevents the binding of RhoA. This mechanism is similar to GEF-H1 interaction with microtubules and cingulin (Ren et al., 1998; Krendel et al., 2002; Aijaz et al., 2005), both known to inhibit GEF-H1–mediated activation of RhoA (Ren et al., 1998; Krendel et al., 2002; Aijaz et al., 2005). Our results, however, ruled out microtubules and cingulin as being responsible for the reduction in GEF-H1 activity.

We previously showed that RhoA destabilized AJs via actomyosin-mediated increase in tension at VE-cadherin

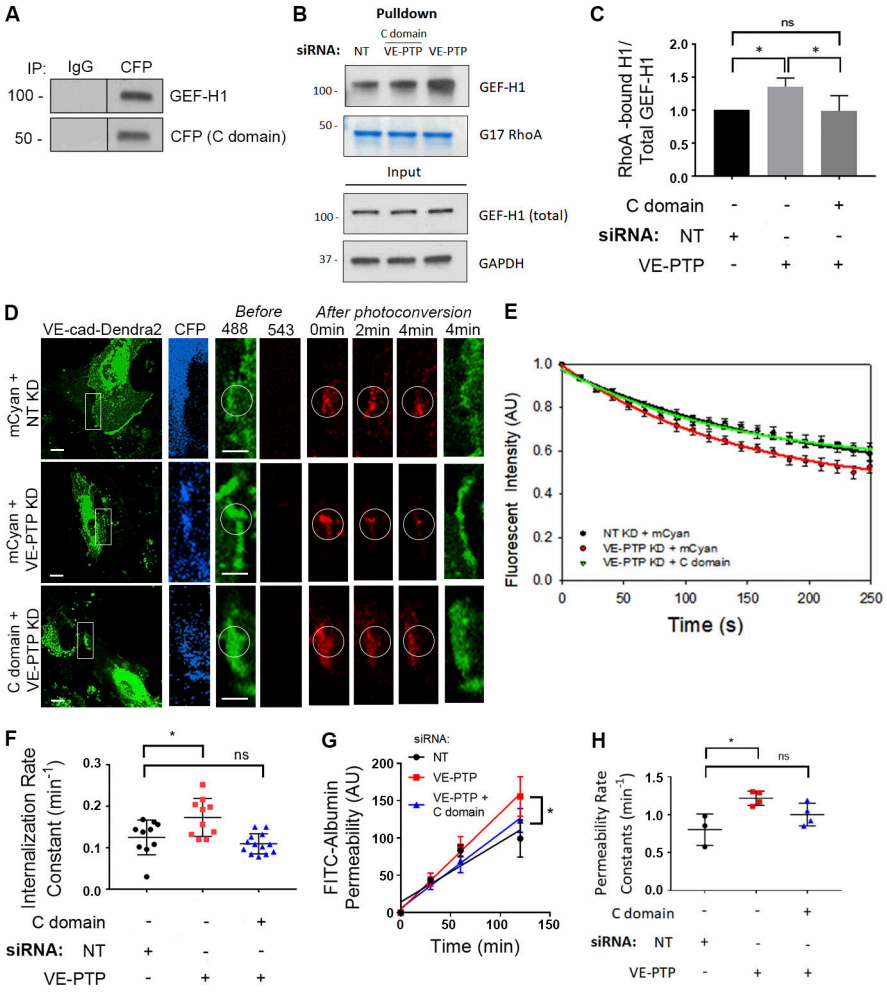

Figure 7. **The VE-PTP cytosolic domain restores the VE-cadherin internalization rate and GEF-H1 activity in VE-PTP–depleted endothelial monolayers. (A)** Immunoprecipitation (IP) of the CFP-tagged VE-PTP C domain from HPAEC lysates. Blots were probed for GEF-H1 and CFP. **(B)** Interaction of GEF-H1 with GST-RhoA (G17A) in HPAECs treated with NT siRNA or depleted of VE-PTP with and without overexpression of the VE-PTP cytosolic (C) domain. The resulting precipitates were probed for GEF-H1. **(C)** Analysis of interaction from data in B; mean ± SEM; $n = 3$; *, $P < 0.05$; one-way ANOVA. **(D)** VE-cad-Dendra2 before (green) and after (red) photoconversion in HPAECs treated with of NT siRNA or VE-PTP siRNA and overexpressing mCyan or HPAECs treated with VE-PTP siRNA and expressing the VE-PTP cytosolic (C) domain. Scale bars, 5 µm. **(E)** VE-cadherin internalization rate curves for groups in D; mean ± SEM; n = 10–13 junctions from three independent experiments. **(F)** Internalization rate constants calculated from E were 0.12 ± 0.01 min^{-1} in NT siRNA–treated cells, 0.17 ± 0.01 min^{-1} in VE-PTP–depleted cells, or 0.11 ± 0.01 min^{-1} in VE-PTP–depleted cells overexpressing the VE-PTP C domain; mean ± SEM; n = 10–13 junctions from three independent experiments; *, $P < 0.05$; one-way ANOVA. **(G)** Permeability of HPAEC monolayers to FITC-conjugated albumin in HPAECs treated with of NT siRNA or VE-PTP siRNA and overexpressing mCyan or HPAECs treated with VE-PTP siRNA and expressing the VE-PTP cytosolic (C) domain; n = 3–4; *, $P < 0.05$; one-way ANOVA. **(H)** Permeability rate constants from G were 0.80 ± 0.12 min^{-1} in NT siRNA-treated cells, 1.22 ± 0.05 min^{-1} in VE-PTP–depleted cells, or 1.00 ± 0.07 min^{-1} in cells overexpressing VE-PTP domain and on the background of VE-PTP depletion; mean ± SEM; n = 3–4; *, $P < 0.05$; one-way ANOVA. KD, knockdown.

adhesions (Yamada and Nelson, 2007; Daneshjou et al., 2015). The RhoA-generated force at junctions was required to disrupt VE-cadherin trans-interactions and promote VE-cadherin internalization (Daneshjou et al., 2015). We also demonstrated that the spatial inhibition of the RhoA–ROCK pathway at AJs reduced the tension and stabilized VE-cadherin junctions (Daneshjou et al., 2015). Here, we describe a VE-PTP–regulated mechanism responsible for inhibiting RhoA signaling at AJs. We showed that VE-PTP's interaction with GEF-H1 at AJs in the quiescent endothelium reduced tension across VE-cadherin junctions. The knockdown of VE-PTP increased the interaction of GEF-H1 with RhoA and also RhoA activity, leading to increased tension across VE-cadherin junctions, whereas overexpression of VE-PTP reduced the tension applied to VE-cadherin junctions secondary to reduced RhoA activity. Overexpression of the VE-PTP PI mutant functioned similarly to WT VE-PTP, indicating that VE-PTP functioned independently of its phosphatase activity. Interestingly, in endothelial monolayers challenged with α-thrombin, full-length VE-PTP itself as opposed to the VE-PTP PI mutant reduced tension, indicating that the mechanism identified in the present studies functions only in the quiescent endothelium. In the activated endothelium, VE-PTP plays a role in dephosphorylating VE-cadherin at Y658 and Y685 and inhibits VE-cadherin internalization to restore endothelial barrier integrity (Gong et al., 2015). The present results support the model that VE-PTP (independent of phosphatase activity) modulates RhoA at AJs to stabilize VE-cadherin junctions through a reduction in actomyosin tension at AJs.

The continuous exchange of VE-cadherin between junctional and cytosolic pools maintains the steady-state homeostasis of AJs (Xiao et al., 2003, 2005; Daneshjou et al., 2015; Dorland et al., 2016; Kruse et al., 2019). We previously established a relationship between tension across VE-cadherin adhesions and VE-cadherin internalization rates at AJs (Daneshjou et al., 2015). Here, we extend this concept by describing a VE-PTP–dependent mechanism providing control of VE-cadherin internalization at AJs in the quiescent endothelium. Knockdown of VE-PTP increased the VE-cadherin internalization rate and endothelial permeability, whereas knockdown of GEF-H1 or overexpression of the cytosolic domain of VE-PTP responsible for the interaction with GEF-H1 restored the VE-cadherin internalization rate and reduced endothelial permeability. While depleting GEF-H1 might have broader effects on endothelial function through reorganization of the actin cytoskeleton (Krendel et al., 2002;

Birukova et al., 2006, 2010), our data demonstrate a fundamental role of GEF-H1 associated with VE-PTP on the stability of VE-cadherin junctions and the basal endothelial barrier. Interestingly, depletion or overexpression of VE-PTP had no effect on Rac1 activity at AJs, suggesting a specific function of VE-PTP in modulating RhoA signaling. While RhoA is implicated in regulating cell–cell adhesion by antagonizing Rac1 signaling in ECs (Wójciak-Stothard et al., 2001; Vouret-Craviari et al., 2002; Shcherbakova et al., 2018), we observed that VE-PTP stabilized VE-cadherin junctions solely through a reduction in RhoA activity.

In conclusion, we demonstrate a novel function of VE-PTP in stabilizing VE-cadherin junctions in the quiescent confluent endothelial monolayer. VE-PTP promotes endothelial barrier stability by reducing the rate of VE-cadherin internalization and restricting endothelial permeability. VE-PTP serves a critical adaptor function through direct interaction with GEF-H1 and inhibits its binding to RhoA, thus reducing RhoA activity and tension at VE-cadherin junctions. This is an essential factor regulating the stability of AJs in vessels.

Materials and methods

DNA constructs

For mammalian expression, VE-cad-Dendra2 was inserted into a pCDNA3 vector (Daneshjou et al., 2015) at 5′-KpnI and 3′-EcoRI restriction sites for VE-cadherin and sites 5′-EcoRI and 3′-XhoI for Dendra2; the FRET-based RhoA and Rac1 biosensors in a pTriEx plasmid with a hybrid promoter (Pertz et al., 2006; MacNevin et al., 2016) were a gift from K. Hahn (University of North Carolina School of Medicine, Chapel Hill, NC). The VE-cadherin tension FRET-based biosensor was in a pLPCX plasmid with a cytomegalovirus (CMV) promoter. The tension sensor module (TSmod) was placed into mouse VE-cadherin cytoplasmic domains (Conway et al., 2013). The human VE-cadherin–GFP adenovirus was in a pAdRSV plasmid with a dL327 backbone and CMV promoter (Shaw et al., 2001). CFP-tagged murine full-length VE-PTP aa 1–1,998 (WT VE-PTP) was cloned from mVE-PTP cDNA (Winderlich et al., 2009), a gift from D. Vestweber (Max Planck Institute for Molecular Biomedicine, Münster, Germany), into pAmCyan1-C1 (catalog number PT3478-5 or 632441; Clontech) at flanking 5′/3′-SalI restriction sites. CFP-tagged deletion mutant VE-PTP aa 1,422–1,998 (Δ16FN) was generated from WT VE-PTP and inserted into pAmCyan1-C1 at 5′-BglII and 3′-EcoRI restriction sites. CFP-tagged deletion mutant VE-PTP aa 1–1,650 (ΔC) and CFP-tagged deletion mutant VE-PTP aa 1,611–1,998 (ΔN) were generated from WT VE-PTP and inserted into pAmCyan1-C1 at 5′-BspEl and 3′-Xhol sites. Plum-tagged deletion mutant VE-PTP aa 1,422–1,998 was generated from CFP-tagged Δ16FN and inserted into pPlum-C1 vector at 5′-BglII and 3′-EcoRI. pPlum-C1 vector was constructed using the pAmCyan1-C1 vector as the backbone, where cDNA for the mPlum protein (catalog number 632527; Clontech) replaced cDNA for the AmCyan1 protein. CFP-tagged VE-PTP PI mutant with a D/A mutation at aa 1,871 was generated from WT VE-PTP using site-directed mutagenesis. CFP-tagged deletion mutant VE-PTP aa 1,651–1,998 was generated from WT VE-PTP and inserted into pAmCyan1-C1 at 5′-BspEI and 3′-XhoI restriction sites. Plum-tagged deletion mutant VE-PTP aa 1,422–1,998 was generated from CFP-tagged Δ16FN and inserted into pPlum-C1 vector at 5′-BglII and 3′-EcoRI.

For bacteria expression and purification, GST-GEF-H1 deletion mutants aa 1–236, aa 237–464, aa 462–570, and aa 570–985 were in pGEX-KG vector (Pathak et al., 2012) and were provided by C. DerMardirossian (The Scripps Research Institute, La Jolla, CA). GST-GEFH1 aa 572–985 was used to generate the panel of GST-GEF-H1 C-terminal constructs (aa 572–876, aa 731–876, aa 731–925, and aa 731–985) by subcloning corresponding regions into pGEX-KG at 5′-EcoRI and 3′-HindIII restriction sites. Histidine-tagged cytoplasmic VE-PTP domain aa 1,651–1,998 was generated by subcloning the cytoplasmic domain (aa 1,651–1,998) of VE-PTP into pNH-TRXT (plasmid 26106; Addgene) at 5′-EcoRI and 3′-HindIII restriction sites. All DNA constructs are listed in Table 1.

Cell culture, transfection, and treatments

Primary human pulmonary arterial endothelial cells (HPAECs) from six different donors were used at passages 3–6 for all experiments. Cells were grown in EBM-2 cell culture medium supplemented with 10% FBS and EGM-2 bullet kit (Lonza) and maintained at 37°C with 5% CO_2. For imaging, HPAECs were plated on gelatin-coated (0.2%) glass-bottom coverslips and transfected at 70–80% confluency with siRNA (200 nM) using Genlantis Transfection Kit. 48 h later, they were transfected with DNA plasmids using X-tremeGENE transfection reagent (Roche). Postconfluent ECs were used for live-cell imaging 24 h after DNA plasmid transfection (72 h after siRNA treatment). In the experiments that did not involve siRNA treatment, the cells were transfected with DNA plasmids at 90% confluence and used for the experiments between 24 and 48 h after transfection (Table 1).

In AKB-9785 studies, HPAECs were treated with different concentrations (0–50 µM) of the inhibitor for 1 h in serum-free media. Cells were either collected for Western blot (ThermoFisher) or imaged immediately after treatment.

To test the role of RhoA activity in VE-cadherin internalization, Rho Activator I CN-01 (50 µM; Cytoskeleton, Inc.) and Rockout (Rho kinase inhibitor, 50 µM) were used to activate or inhibit the Rho pathway, respectively.

To test the phospho-profile of VE-cadherin in the presence of the various VE-PTP constructs, CHO cells were infected with GFP-VE-cadherin and transfected with the VE-PTP construct simultaneously. The resulting lysates were analyzed with Western blot and probed with VE-cadherin (anti-goat; sc-6458; Santa Cruz) and VE-cadherin phospho-tyrosine antibodies for Tyr658 (anti-rabbit; 44-1144G; ThermoFisher) and Tyr685 (anti-rabbit; ab119785; Abcam).

Immunostaining

HPAEC postconfluent monolayers were stained as previously described (Kruse et al., 2019). Briefly, cells were washed with warm HBSS buffer containing both Ca^{2+} and Mg^{2+}, fixed with 4% formaldehyde or a mixture of 4% formaldehyde and 0.1% glutaraldehyde (for tubulin staining) for 15 min at room temperature, permeabilized with 0.1% Triton X-100 for 15 min, and

Table 1. **Lists of reagents used in experiments**

Cell lines and reagents	Company	Catalog number and sequences
Cell lines		
HPAECs	Lonza	cc-2530 (lot numbers 329447, 447095, 466719, 598033, 662151, 4F3034)
CHO-K1	ATCC	TCC CCL-61
Antibodies		
Phosphotyrosine antibody (PY20)	Abcam	ab16389
Phosphotyrosine antibody, clone 4G10	EMD Millipore	05-321X
VE-cadherin antibody	Santa Cruz	sc-6458
Phospho-VE-cadherin (Tyr685)	EMD Millipore	ABT1760
Phospho-VE-cadherin (Tyr658) polyclonal antibody	ThermoFisher	44-1144G
Phospho-VE-cadherin (Tyr685) polyclonal antibody	Abcam	ab119785
Phospho-VE-cadherin (Tyr731) Polyclonal antibody	ThermoFisher	44-1145G
TIE2 antibody	Abcam	ab58302
human/mouse phospho-Tie-2 (Y992) antibody	R&D Systems	AF2720
Cingulin polyclonal antibody	Novus Biologicals	NBP1-89602
GEF-H1 antibody	Abcam	ab155785
Anti–GEF-H1 antibody [B4/7]	Abcam	ab90783
p114RhoGEF (ARHGEF18) monoclonal antibody	Novus Biologicals	NBP2-43546
p115RhoGEF (D-11; ARHGEF1) monoclonal antibody	Santa Cruz	sc-166341
RGNEF (ARHGEF28) polyclonal antibody	Abcam	ab157095
GST antibody (A-6)	Santa Cruz	sc-374171
6x-His Tag monoclonal antibody	ThermoFisher	4E3D10H2/E3
GFP Tag monoclonal antibody	ThermoFisher	GF28R
PTPβ antibody (C-20)	Santa Cruz	sc-1114
RPTPβ antibody	BD Biosciences	610180
Alexa Fluor 488 Phalloidin	Invitrogen	A12379
Mouse monoclonal anti-β-tubulin	Sigma Aldrich	T8328
Anti-mouse IgG (Fc) antibody	Aviva Systems Biology	OARD00003
Primers		
pNH-TRXT-VE-PTP aa 1,651–1,998-6xHis	Integrated DNA Technologies	VE-PTP aa 1,651 EcorRI Fwd; 5′-ATAGGAGAATTCGCCACC ATGAGGGAAAGGCCATCTGCC-3′
		VE-PTP aa 1,998 HindIII Rev; 5′-AAACCTAAGCTTATGTCT CGAGTAGATTGC-3′
mPlum VE-PTP 1,422–1,998 D1871A	Integrated DNA Technologies	VE-PTP D1871A Fwd 5′-GCCAGCCCATGGGGTCCCAGAG-3′
		VE-PTP D1871A Rev 5′-CCATGGGCTGGCCACACCGTGT-3′
mPlum VE-PTP 1,611–1,998	Integrated DNA Technologies	VE-PTP 1,611 BspEI Fwd 5′-AGCGCGTCCGGAGCCACCATG ACCACAGAGTCAGAGCCCTTGTTTGGAG-3′
		VE-PTP 1,998 XhoI Rev 5′-GCCGCCTCTAGACTAATGTCT CGAGTAGATTGCATCTCTGTGATAC-3′
pAmCyan VE-PTP 1,651–1,998	Integrated DNA Technologies	VE-PTP 1,651 BspEI Fwd 5′-GACACGTCCGGAGCCACCATG AGGGAAAGGCCATCTGCCCGGCTCAGC-3′
		VE-PTP 1,998 XhoI Rev 5′-GGGCCCCTCGAGTTAATGTCT CGAATAGATTGCATCTCTGTGATACTC-3′
mPlum VE-PTP 1–1,650	Integrated DNA Technologies	VE-PTP 1 BspEI 5′ Fwd 5′-AGCGCGTCCGGAGCCACCATG CTGAGGCATGGAGCCCTAACGGCCTTG-3′
		VE-PTP 1,650 XhoI Rev 5′-GCCGCCCTCGAGGCTAGCTTT CTGTCTGCAGATGAAGAAGGC-3′

Table 1. **Lists of reagents used in experiments (*Continued*)**

Cell lines and reagents	Company	Catalog number and sequences
GST-GEFH1 572–876	Integrated DNA Technologies	GEFH1 572 EcoRI Fwd 5′-GGACTCGAATTCGAGCCACCATGA CATGCCCATCCAGGGAGGAC-3′
		GEFH1 876 HindIII Rev 5′-AGGTCCAAGCTTTTAATCCACAGG TCTGCGGGCCCA-3′
GST-GEFH1 731–985	Integrated DNA Technologies	GEFH1 731 EcoRI Fwd 5′-GGACTCGAATTCGAGCCACCATGA GATCACCGCAAGAGGAGGCG-3′
		GEFH1 985 HindIII Rev 5′-AGGTCCAAGCTTTTAGCTCTCGGA GGCTACAGCCTC-3′
GST-GEFH1 731–876	Integrated DNA Technologies	GEFH1 731 EcoRI Fwd 5′-GGACTCGAATTCGAGCCACCATGA GATCACCGCAAGAGGAGGCG-3′
		GEFH1 876 HindIII REV 5′-AGGTCCAAGCTTTTAATCCACAGG TCTGCGGGCCCA-3′
GST-GEFH1 731–925	Integrated DNA Technologies	GEFH1 731 EcoRI Fwd 5′-GGACTCGAATTCGAGCCACCATGA GATCACCGCAAGAGGAGGCG-3′
		GEFH1 925 HindIII Rev 5′-AGGTCCAAGCTTTTACCCCAGTTC CTGCCTCTCTCG-3′
pAmCyan-VE-PTP 1,611–1,998	Integrated DNA Technologies	VE-PTP 1,611 BspEI Fwd 5′-AGCGCGTCCGGAGCCACCATG ACCACAGAGTCAGAGCCCTTGTTTGGAG-3′
		VE-PTP 1,998 XhoI Rev 5′-GCCGCCTCTAGACTAATGTCT CGAGTAGATTGCATCTCTGTGATAC-3′
pAmCyan-VE-PTP 1–1,650	Integrated DNA Technologies	VEPTP 1 BspEI Fwd 5′-AGCGCGTCCGGAGCCACCATGCTG AGGCATGGAGCCCTAACGGCCTTG-3′
		VEPTP 1,650 XhoI Rev 5′-GCCGCCCTCGAGGCTAGCTTTCTG TCTGCAGATGAAGAAGGC-3′
Plasmids		
mPlum-C1	Clontech	632527
pAmCyan1-C1	Clontech	632441
pNH-TrxT	Addgene	26106
VE-cad-Dendra2	Daneshjou et al., 2015	N/A
VE-cadherin-GFP	Shaw et al., 2001	N/A
VE-cadherin tension FRET biosensor	Conway et al., 2013	N/A
pTriEx-Rac1 FLARE.dc biosensor WT	MacNevin et al., 2016	N/A
pTriEx-RhoA FLARE.sc biosensor WT	Pertz et al., 2006	Addgene: 12150
siRNA target sequences		
ON-TARGETplus ARHGEF2 siRNA	Dharmacon	J-009883-09; 5′-CCACGGAACUGGCAUUACU-3′
ON-TARGETplus Human ARHGEF1 siRNA SMARTpool	Dharmacon	J-009421;
		1. 5′-UGACGUGGCGGGUGACUAA-3′,
		2. 5′-AAACYGGUGUGCUCUCAUC-3′,
		3. 5′-5′-CCACGGCCCUUCGGAAAGU-3′,
		4. 5′-UAUACGAGCUGGUGGCACA-3′
ON-TARGETplus human ARHGEF18 siRNA SMARTpool	Dharmacon	J-009654;
		1. 5′-UCAGGGCGCUUGAAAGAUA-3′,
		2. 5′-GCAGUGACCGGAAUUAUGU-3′,
		3. 5′-CACAACGCAUAACCAAAUA-3′,
		4. 5′-GGACGCAACUCGGACCAAU

Table 1. **Lists of reagents used in experiments (*Continued*)**

Cell lines and reagents	Company	Catalog number and sequences
ON-TARGETplus human ARHGEF28 siRNA SMARTpool	Dharmacon	J-024506;
		1. 5′-CAAGUAAUCUACAGUCGAA-3′,
		2. 5′-CAUAAAGACUUACGCAAAG-3′,
		3. 5′-GGCUUGAGAUCCUAAAUAA-3′,
		4. 5′-GAAGAUAUAAAGCGUGUCA-3′
ON-TARGETplus PTPRB siRNA	Dharmacon	J-004994-07; 5′-GAUCUAACAUUGCGCAACA-3′
siGENOME NT siRNA pool	Dharmacon	D-001206-13
Reagents		
X-tremeGENE HP DNA transfection reagent	Sigma Aldrich	6366244001
Gene silencer transfection reagent	Genlantis	T500750
Pierce Protein G Agarose	ThermoFisher	20398
Protein A/G PLUS-Agarose	Santa Cruz	sc-2003
RhoA G17A Agarose beads	Abcam	ab211183
Human α-thrombin	Enzyme Research Laboratories	HT 5142
ROCK inhibitor III	Santa Cruz	sc-203237
RhoA activator I	Cytoskeleton, Inc.	CN01
QC colloidal Coomassie stain	BioRad	1610803

Antibodies, reagents, primers, cell lines, siRNA, and vectors used in experiments throughout this study. Company, catalog numbers, and sequences (if applicable) are indicated. Fwd, forward; N/A, not applicable; Rev, reverse.

blocked using 3% BSA for 1 h. The samples were incubated with primary antibodies against the protein of interest (VE-cadherin [anti-goat; sc-6458; Santa Cruz]; cingulin [anti-rabbit; NBP1-89602; Novus Biologicals]; GEF-H1 [anti-mouse; ab90783; Abcam]; tubulin [anti-mouse; T8328; Sigma Aldrich]) or Alexa Fluor 647 phalloidin at 1:100 overnight at 4°C and thereafter with secondary antibodies 1:100 at room temperature for 1 h. Cells were mounted using Fluoromount-G (Southern Biotech).

Immunostaining analysis

To analyze VE-cadherin, GEF-H1, and cingulin at AJs, a Z-projected image (maximum intensity) of the in-focus frames were generated. VE-cadherin junctional area was measured using a threshold function to select only junctional VE-cadherin. VE-cadherin thresholded images were also used to generate a binary mask in order to determine the area and average intensity (accumulation) of GEF-H1 and cingulin at AJs. The VE-cadherin mask was multiplied by the GEF-H1 or cingulin channels to remove any nonjunctional protein.

For analyses of microtubules and actin cytoskeleton, a Z-projected images (maximum intensity) of the in-focus frames for either the microtubules or the actin were generated. The total areas of either microtubules or actin were measured using thresholded images. The total microtubule or actin areas were normalized to the cell area.

Live-cell imaging

HPAECs were imaged in phenol red–free EGM-2 media supplemented with 10% FBS and heated on a stage heater (Temp control 37°C; Carl Zeiss) at 37°C. Time-lapse images were generated using an LSM 710 confocal microscope (Carl Zeiss) containing a 63×, 1.4-NA oil-immersion objective lenses and Ar ion and dual HeNe lasers. Image analysis was done using Metamorph software and images were prepared using Adobe Photoshop.

To study VE-cadherin dynamics, HPAECs coexpressing VE-cad-Dendra2 and CFP-tagged VE-PTP were simultaneously imaged in green (λ = 488 nm) and red (λ = 543 nm) fluorescent states of Dendra2. VE-cad-Dendra2 undergoes an emission shift from 488 nm (green) to 543 nm (red) after irradiation using a 405-nm laser at 8–12% power (Daneshjou et al., 2015; Kruse et al., 2019). Images were acquired every 5 s. Through the analysis of red fluorescent decay and green fluorescent recovery within a circular irradiation zone, we determined the rates of VE-cadherin internalization from the AJ and the recruitment of VE-cadherin molecules to the AJ, respectively. The AJs exhibiting a slower VE-cadherin internalization rate were considered to be more stable. For FRET imaging, 16-bit z-stack images were acquired for CFP (λ = 458 nm; band pass 500/20 nm), FRET (λ = 458 nm; long pass 530 nm), and YFP (λ = 514 nm; long pass 530 nm) as previously described (Daneshjou et al., 2015; Kruse et al., 2019).

Image processing

In VE-cad-Dendra2 studies, the fluorescent intensities of 488-nm (green) and 543-nm (red) maximum emission spectra were quantified inside the photoconversion zone. The changes in fluorescent integrated intensities over time were analyzed in

Metamorph. Data obtained in Metamorph were fit to exponential decay and exponential rise-to-maximum curves for red and green fluorescence, respectively, in Sigmaplot. Rate constants were calculated from exponential curves and signify VE-cadherin internalization (at 543 nm) and recruitment (at 488 nm).

FRET processing was performed in either Metamorph or ImageJ. A binary mask was generated using a maximized and thresholded image of YFP z-stack, where outside the cell fluorescence has a value of 0 and inside the cell has a value of 1. A ratio image (FRET/CFP) was created by separately multiplying the FRET and CFP z-stack images by the YFP binary mask. FRET was then divided by CFP to generate a ratio. The region used for quantification consisted of a thick area between two ECs (i.e., junction and overlapping membrane). The activity of RhoA and the tension applied to VE-cadherin were expressed as a FRET/CFP ratio.

Protein purification

His-tagged VE-PTP and GST-tagged GEF-H1 constructs were transformed into BL21-competent bacterial cells. Proteins were induced with IPTG for 4 h at 30°C. Bacterial pellets were resuspended and lysed (50 mM Tris, 150 mM NaCl, and 5 mM imidazole, pH 7.5) before incubation with NiNTA-His beads or GST beads for 1 h. Proteins were purified using column purification. Expression of purified protein was confirmed on Coomassie-stained SDS gel.

Binding assay

To confirm direct binding between VE-PTP and GEF-H1, a binding assay was performed. Briefly, binding buffers containing 20 mM Tris-HCl, pH 7.5, 100 mM, 1 mM mercaptoethanol, and 1% Triton X-100 (Lansbergen et al., 2004) were used for binding assay experiments. 10 µg GST-tagged GEF-H1 and 10 µg His-tagged VE-PTP purified proteins were incubated with binding buffer at 4°C for 90 min. His-tagged VE-PTP was pulled down using HisPur Ni-NTA beads, run on SDS-PAGE, and probed with GST (anti-mouse; sc-374171; Santa Cruz) or His antibody (anti-mouse; 4E3D10H2/E3; ThermoFisher).

Mass spectrometry analysis

To determine VE-PTP binding partners, CFP-VE-PTP was overexpressed in HPAECs and an immunoprecipitation was performed using an anti-GFP antibody (anti-mouse; GF28R; ThermoFisher). The resulting precipitates were run on an SDS gel, stained with Coomassie, and analyzed using proteomic analysis (Harvard Medical School Taplin Mass Spectrometry Facility).

RhoA G17A pull-down assay

The level of GEF-H1 activity was determined as previously described (Kruse et al., 2019). 1 ml HPAEC lysates from cells treated with siRNA or overexpressing DNA construct was incubated with 40 µl nucleotide-free GST-tagged RhoA G17A attached to beads (ab211183; Abcam) for 2 h. The beads were centrifuged and washed three times in lysis buffer. Captured proteins on RhoA G17A beads were separated by electrophoresis and detected with GEF-H1 antibody (anti-rabbit; ab155785; Abcam) using Western blot.

Cell isolation and modification

The surfaces of the erythrocytes used to probe the cadherin-mediated adhesion were covalently modified with oriented, immunoglobulin Fc-tagged ectodomains of human VE-cadherin. The erythrocytes were isolated from human whole blood collected from healthy subjects by informed consent. The erythrocyte surfaces were modified with either anti-Fc or anti-hexahistidine antibodies, as described previously (Kofler and Wick, 1977). The immobilized antibodies were used to capture Fc-tagged or hexahistidine-tagged VE-cadherin ectodomains.

MLECs were isolated from the lungs of WT *VE-PTP*$^{flox/flox}$ mice and *VE-PTP*$^{-/-}$ KO mice as previously described (Quaggin, 2017). VE-PTP KO transgenic mice exhibited the following genotype: *PTPRB*$^{flox/flox}$, *rosa26rtTA*$^{+/+}$, *tetOCre*$^{+/-}$. *PTPRB* gene encoding VE-PTP was deleted in utero by adding tetracycline to the drinking water starting at embryonic day 13.

Interaction of RBCs with VE-cadherin ectodomains

C-terminal Fc-tagged E-cadherin ectodomains were bound and oriented on RBCs modified with anti-Fc antibody (Aviva Systems Biology), respectively.

Quantification of VE-cadherin surface expression

Flow cytometry measurements were used to measure the VE-cadherin densities on cell surfaces (cadherin/per square micrometer; Chien et al., 2008). VE-cadherin–expressing cells were labeled with primary, anti-VE-cadherin antibody. The secondary antibody is FITC-conjugated anti-IgG. The antibody labeling was done in PBS containing 1% BSA at pH 7.4. Calcium was removed at this step in order to prevent cell aggregation. The fluorescence intensities of labeled cells were measured with an LSR II flow cytometer (BD Biosciences). The calibration curve for the fluorescence intensity was generated with calibrated FITC-labeled beads (Bands Laboratories).

Micropipette measurement of cell-binding kinetics

Adhesion frequency measurements quantified the intercellular binding probability as a function of cadherin contact time by using opposing micropipettes to control interacting cell pairs (Fig. S1 I). The recorded binding probability, P(t), is the ratio of the number of binding events (nb) to the total cell–cell touches (NT), nb/NT; this is a function of number of cell-to-cell bonds. In these measurements, a VE-cadherin–expressing cell and a RBC with surface-bound, His-tagged VE-cadherin ectodomain were partially aspirated into opposing glass micropipettes (Fig. S1 I). The experimental chamber contained L15 medium (Invitrogen) supplemented with 1 wt/vol% BSA and 2 mM $CaCl_2$ and diluted 1:1 with deionized water. This hypo-osmotic solution keeps the RBC rounded. Cells were observed with a 100× oil-immersion objective on a Zeiss Axiovert 200 microscope, and images were recorded with a Manta G201B camera (AVT Technologies) interfaced with a high-resolution (1,080 × 720 pixels), flat-screen monitor. The contact time was manipulated with automated piezoelectric controllers programmed to repeatedly bring the two cells into contact for defined time intervals. The contact area was controlled at 6 ± 1 µm^2 during a set of measurements. Binding events were identified from surface deformation of the

RBCs during separation and the recoil at bond failure. Each cell pair was tested for 50 repetitive cell–cell touches (NT = 50), and each contact time represents measurements with at least three different cell pairs. The mean and standard error of each set of 50 tests was determined from the Bernoulli distribution. The probabilities (P) shown in the graphs are the average of measurements with at least three cell pairs, and error bars indicate the standard error of the three sets of measurements with different cell pairs at each time point.

The analytical expression for the time-dependent binding probability, $P(t)$, for the reaction is as follows: $P(t) = 1 - exp(-\{mRmLAcK2D[1 - exp(-k_{off}t)]\})$, where mL and mR are the receptor and ligand surface densities (number per square micrometer) on two cells, Ac is the contact area (μm^2), $K2D$ is the two-dimensional binding affinity (μm^2), and k_{off} is the off rate (s^{-1}). The ligand densities (number per square micrometer) and contact areas are known. The two-dimensional affinity $K2D$ and k_{off} for trans-dimerization were then estimated from fits of the above equation to the data corresponding to the first, trans-binding step (i.e., the rise to P1; Chesla et al., 1998).

Micropillar arrays

The micropillar methodology was used to quantify the imbalance in cellular traction forces when cells are in a cluster. Because the net force on the cell must be zero, the traction force must be balanced with the tension on cell junctions. The micropillar enables definition of the exact forces at the cell junction, whereas the FRET biosensor provides a relative indication of changes in force.

VE-PTP$^{flox/flox}$ (WT) and *VE-PTP*$^{-/-}$ (KO) MLECs were immunofluorescent stained by permeabilization with 0.1% (vol/vol) Triton X-100 in PBS for 4 min and blocked with 1% (wt/vol) bovine serum albumin in PBS for 1 h. Cells were incubated with β-catenin primary and then with secondary antibodies for 1 h at room temperature (1:40 dilution; catalog number C7207; Sigma Aldrich; goat anti-mouse IgG Alexa Fluor 488, 1:200 dilution; Life Technologies). Samples were mounted with Fluoromount G onto micropillars stained with DiD and coated with fibronectin and stored at 4C until imaging. Images of the micropillar tip positions and endothelial junctions were taken on a Zeiss Axiovert.Z1 epifluorescence microscope with a 40× oil immersion objective (Institute for Genomic Biology, University of Illinois at Urbana-Champaign). Mechanical force calculations were only done using cell doublets and linear triplets.

Junction area was calculated using ImageJ v1.51k (National Institutes of Health) from β-catenin immunostaining. Traction force analysis was performed using a custom MATLAB program written for MATLAB R2007a (Cohen et al., 2013).

The traction force map was calculated using beam bending theory for small cantilever deflections: $F = k \times x$; $k = (3EI/L^3)$; $I = (\pi d^4/64)$, where F is the force exerted on the free end of the cantilever, k is the spring constant, x is the deflection, E is the bulk elastic modulus, I is the area moment of inertia, L is the length of the cantilever, and d is the diameter of the cantilever. Knowing the displacement (x) map and the spring constant (22 nN), a traction force (F) map can be generated.

The junction stress for each junction was calculated with the equation, where junction area is calculated from β-catenin immunostaining. Dividing cell junction tension by cell junction area provides a measure of stress at cell junctions (stress = force/area). This stress is the force acting on a unit element of cell junction, and the readout is equivalent to the tension from the FRET biosensor.

Traction force microscopy

Traction force microscopy measurements used polyacrylamide hydrogels with Young's moduli 40 kPa (Tse and Engler, 2010). Proteins were immobilized on Sulfo-SANPAH–activated gels by overnight incubations at 4°C with fibronectin (0.1 mg/ml) or PLL (0.2 mg/ml) in immobilization buffer (100 mM Hepes, 100 mM NaCl, and 5 mM $CaCl_2$, pH 8; Tabdili et al., 2012). The substrates were rinsed twice with 1× PBS and sterilized by irradiation (365 nm) for at least 15 min before seeding cells. MLECs were harvested using 3.5 mM EDTA in PBS containing 1% (wt/vol) BSA (Takeichi and Nakagawa, 2001), seeded at 5,000–8,000 cells/ml onto hydrogels, and allowed to adhere and spread for 6 h at 37°C under 5% CO_2 on polyacrylamide gels with embedded fluorescent microspheres. The absolute basal root mean square traction force was determined from fiduciary bead displacements, relative to the traction-free bead positions after cell removal (lysis; Butler et al., 2002). Constrained traction maps and the root mean square traction stress (Pa; N/m^2) were determined from the bead displacement maps (Butler et al., 2002).

Statistical analysis

Statistical significance was analyzed using GraphPad Prism. Unpaired *t* tests were performed for two experimental groups, and one-way ANOVA was performed for three or more experimental groups. The following P values are used: *, $P < 0.05$; **, $P < 0.01$; *** $P < 0.001$.

Online supplemental material

Fig. S1 shows that VE-PTP stabilizes AJs by reducing the VE-cadherin internalization rate, but not via VE-cadherin recruitment or trans-dimerization, in the quiescent endothelium (related to Figs. 1 and 2). Fig. S2 shows that inhibition of VE-PTP phosphatase activity with AKB-9785 fails to prevent the VE-cadherin internalization rate at AJs (related to Figs. 1 and 2). Fig. S3 shows that VE-PTP binds to GEF-H1 and stabilizes VE-cadherin junctions (related to Figs. 3 and 4). Fig. S4 shows that VE-PTP relieves tension across VE-cadherin junctions by inhibiting RhoA signaling (related to Figs. 4 and 5). Fig. S5 shows the relative contributions of RhoGEFs and Rho signaling in regulating the VE-cadherin internalization rate.

Acknowledgments

We thank Dr. Celine DerMardirossian for GEF-H1 plasmids, Tiffany Sharma (University of Illinois at Chicago, Chicago, IL) for constructing VE-PTP constructs, Dr. Klaus Hahn for the RhoA biosensor, Dr. Dietmar Vestweber for the WT VE-PTP construct and thoughtful comments, Dr. Susan E. Quaggin (Northwestern University, Evanston, IL) for lung tissue from *VE-PTP*$^{-/-}$ knockout and control mice, Aerpio Pharmaceuticals

(Cincinnati, OH) for VE-PTP inhibitor AKB-9785, the Taplin Mass Spectrometry Facility (Harvard University), and the University of Illinois Research Resource Center (Core Imaging Facility, University of Illinois College).

This work was supported by National Institutes of Health grants to V.V. Juettner (T32 HL07829), Y. Kahn (R01 HL103922), and A.B. Malik (P01 HL60678 and R01HL45638).

The authors declare no competing financial interests.

Author contributions: A.B. Malik, Y.A. Komarova, and V.V. Juettner conceived the project, interpreted data, and wrote the manuscript. V.V. Juettner performed all of the experiments, except those specifically attributed to other authors. K. Kruse performed immunofluorescent staining and analysis, A. Dan performed micropillar array assays, V. Vu performed traction force microscopy, Y. Kahn generated VE-PTP deletion constructs for mammalian and bacterial expression, J. Le performed Western blot, and A.B. Malik, Y. Komarova, and D. Leckband provided critical discussion of the project.

Submitted: 27 July 2018
Revised: 20 December 2018
Accepted: 12 March 2019

References

Abiko, H., S. Fujiwara, K. Ohashi, R. Hiatari, T. Mashiko, N. Sakamoto, M. Sato, and K. Mizuno. 2015. Rho guanine nucleotide exchange factors involved in cyclic-stretch-induced reorientation of vascular endothelial cells. *J. Cell Sci.* 128:1683–1695. https://doi.org/10.1242/jcs.157503

Aijaz, S., F. D'Atri, S. Citi, M.S. Balda, and K. Matter. 2005. Binding of GEF-H1 to the tight junction-associated adaptor cingulin results in inhibition of Rho signaling and G1/S phase transition. *Dev. Cell.* 8:777–786. https://doi.org/10.1016/j.devcel.2005.03.003

Alonso, A., J. Sasin, N. Bottini, I. Friedberg, I. Friedberg, A. Osterman, A. Godzik, T. Hunter, J. Dixon, and T. Mustelin. 2004. Protein tyrosine phosphatases in the human genome. *Cell.* 117:699–711. https://doi.org/10.1016/j.cell.2004.05.018

Baumeister, U., R. Funke, K. Ebnet, H. Vorschmitt, S. Koch, and D. Vestweber. 2005. Association of Csk to VE-cadherin and inhibition of cell proliferation. *EMBO J.* 24:1686–1695. https://doi.org/10.1038/sj.emboj.7600647

Birkenfeld, J., P. Nalbant, B.P. Bohl, O. Pertz, K.M. Hahn, and G.M. Bokoch. 2007. GEF-H1 modulates localized RhoA activation during cytokinesis under the control of mitotic kinases. *Dev. Cell.* 12:699–712. https://doi.org/10.1016/j.devcel.2007.03.014

Birukova, A.A., D. Adyshev, B. Gorshkov, G.M. Bokoch, K.G. Birukov, and A.D. Verin. 2006. GEF-H1 is involved in agonist-induced human pulmonary endothelial barrier dysfunction. *Am. J. Physiol. Lung Cell. Mol. Physiol.* 290:L540–L548. https://doi.org/10.1152/ajplung.00259.2005

Birukova, A.A., P. Fu, J. Xing, B. Yakubov, I. Cokic, and K.G. Birukov. 2010. Mechanotransduction by GEF-H1 as a novel mechanism of ventilator-induced vascular endothelial permeability. *Am. J. Physiol. Lung Cell. Mol. Physiol.* 298:L837–L848. https://doi.org/10.1152/ajplung.00263.2009

Breviario, F., L. Caveda, M. Corada, I. Martin-Padura, P. Navarro, J. Golay, M. Introna, D. Gulino, M.G. Lampugnani, and E. Dejana. 1995. Functional properties of human vascular endothelial cadherin (7B4/cadherin-5), an endothelium-specific cadherin. *Arterioscler. Thromb. Vasc. Biol.* 15:1229–1239. https://doi.org/10.1161/01.ATV.15.8.1229

Broermann, A., M. Winderlich, H. Block, M. Frye, J. Rossaint, A. Zarbock, G. Cagna, R. Linnepe, D. Schulte, A.F. Nottebaum, and D. Vestweber. 2011. Dissociation of VE-PTP from VE-cadherin is required for leukocyte extravasation and for VEGF-induced vascular permeability in vivo. *J. Exp. Med.* 208:2393–2401. https://doi.org/10.1084/jem.20110525

Butler, J.P., I.M. Tolić-Nørrelykke, B. Fabry, and J.J. Fredberg. 2002. Traction fields, moments, and strain energy that cells exert on their surroundings. *Am. J. Physiol. Cell Physiol.* 282:C595–C605. https://doi.org/10.1152/ajpcell.00270.2001

Chesla, S.E., P. Selvaraj, and C. Zhu. 1998. Measuring two-dimensional receptor-ligand binding kinetics by micropipette. *Biophys. J.* 75:1553–1572. https://doi.org/10.1016/S0006-3495(98)74074-3

Chiasson, C.M., K.B. Wittich, P.A. Vincent, V. Faundez, and A.P. Kowalczyk. 2009. p120-catenin inhibits VE-cadherin internalization through a Rho-independent mechanism. *Mol. Biol. Cell.* 20:1970–1980. https://doi.org/10.1091/mbc.e08-07-0735

Chien, Y.H., N. Jiang, F. Li, F. Zhang, C. Zhu, and D. Leckband. 2008. Two stage cadherin kinetics require multiple extracellular domains but not the cytoplasmic region. *J. Biol. Chem.* 283:1848–1856. https://doi.org/10.1074/jbc.M708044200

Chudakov, D.M., S. Lukyanov, and K.A. Lukyanov. 2007. Using photoactivatable fluorescent protein Dendra2 to track protein movement. *Biotechniques.* 42:553–563: 555: 557 passim. https://doi.org/10.2144/000112470

Cohen, D.M., M.T. Yang, and C.S. Chen. 2013. Measuring cell-cell tugging forces using bowtie-patterned mPADs (microarray post detectors). *Methods Mol. Biol.* 1066:157–168. https://doi.org/10.1007/978-1-62703-604-7_14

Conway, D.E., M.T. Breckenridge, E. Hinde, E. Gratton, C.S. Chen, and M.A. Schwartz. 2013. Fluid shear stress on endothelial cells modulates mechanical tension across VE-cadherin and PECAM-1. *Curr. Biol.* 23:1024–1030. https://doi.org/10.1016/j.cub.2013.04.049

Corada, M., L. Zanetta, F. Orsenigo, F. Breviario, M.G. Lampugnani, S. Bernasconi, F. Liao, D.J. Hicklin, P. Bohlen, and E. Dejana. 2002. A monoclonal antibody to vascular endothelial-cadherin inhibits tumor angiogenesis without side effects on endothelial permeability. *Blood.* 100:905–911. https://doi.org/10.1182/blood.V100.3.905

Daneshjou, N., N. Sieracki, G.P. van Nieuw Amerongen, D.E. Conway, M.A. Schwartz, Y.A. Komarova, and A.B. Malik. 2015. Rac1 functions as a reversible tension modulator to stabilize VE-cadherin trans-interaction. *J. Cell Biol.* 209:181. https://doi.org/10.1083/jcb.20140910803202015c

Davidson, D., and A. Veillette. 2001. PTP-PEST, a scaffold protein tyrosine phosphatase, negatively regulates lymphocyte activation by targeting a unique set of substrates. *EMBO J.* 20:3414–3426. https://doi.org/10.1093/emboj/20.13.3414

Del Vecchio, P.J., A. Siflinger-Birnboim, J.M. Shepard, R. Bizios, J.A. Cooper, and A.B. Malik. 1987. Endothelial monolayer permeability to macromolecules. *Fed. Proc.* 46:2511–2515.

Dorland, Y.L., T.S. Malinova, A.M. van Stalborch, A.G. Grieve, D. van Geemen, N.S. Jansen, B.J. de Kreuk, K. Nawaz, J. Kole, D. Geerts, et al. 2016. The F-BAR protein pacsin2 inhibits asymmetric VE-cadherin internalization from tensile adherens junctions. *Nat. Commun.* 7:12210. https://doi.org/10.1038/ncomms12210

Esser, S., M.G. Lampugnani, M. Corada, E. Dejana, and W. Risau. 1998. Vascular endothelial growth factor induces VE-cadherin tyrosine phosphorylation in endothelial cells. *J. Cell Sci.* 111:1853–1865.

Fachinger, G., U. Deutsch, and W. Risau. 1999. Functional interaction of vascular endothelial-protein-tyrosine phosphatase with the angiopoietin receptor Tie-2. *Oncogene.* 18:5948–5953. https://doi.org/10.1038/sj.onc.1202992

Feng, D., J.A. Nagy, K. Pyne, H.F. Dvorak, and A.M. Dvorak. 1998. Neutrophils emigrate from venules by a transendothelial cell pathway in response to FMLP. *J. Exp. Med.* 187:903–915. https://doi.org/10.1084/jem.187.6.903

Fujishiro, S.H., S. Tanimura, S. Mure, Y. Kashimoto, K. Watanabe, and M. Kohno. 2008. ERK1/2 phosphorylate GEF-H1 to enhance its guanine nucleotide exchange activity toward RhoA. *Biochem. Biophys. Res. Commun.* 368:162–167. https://doi.org/10.1016/j.bbrc.2008.01.066

Fujita, S., R.K. Puri, Z.X. Yu, W.D. Travis, and V.J. Ferrans. 1991. An ultrastructural study of in vivo interactions between lymphocytes and endothelial cells in the pathogenesis of the vascular leak syndrome induced by interleukin-2. *Cancer.* 68:2169–2174. https://doi.org/1002/1097-0142(19911115)68:10<2169::AID-CNCR2820681014>3.0.CO;2-F

Gavard, J., and J.S. Gutkind. 2006. VEGF controls endothelial-cell permeability by promoting the beta-arrestin-dependent endocytosis of VE-cadherin. *Nat. Cell Biol.* 8:1223–1234. https://doi.org/10.1038/ncb1486

Gebbink, M.F., O. Kranenburg, M. Poland, F.P. van Horck, B. Houssa, and W.H. Moolenaar. 1997. Identification of a novel, putative Rho-specific GDP/GTP exchange factor and a RhoA-binding protein: control of neuronal morphology. *J. Cell Biol.* 137:1603–1613. https://doi.org/10.1083/jcb.137.7.1603

Gong, H., X. Gao, S. Feng, M.R. Siddiqui, A. Garcia, M.G. Bonini, Y. Komarova, S.M. Vogel, D. Mehta, and A.B. Malik. 2014. Evidence of a common mechanism of disassembly of adherens junctions through Gα13 targeting of VE-cadherin. *J. Exp. Med.* 211:579–591. https://doi.org/10.1084/jem.20131190

Gong, H., J. Rehman, H. Tang, K. Wary, M. Mittal, P. Chaturvedi, Y.Y. Zhao, Y. A. Komarova, S.M. Vogel, and A.B. Malik. 2015. HIF2α signaling inhibits adherens junctional disruption in acute lung injury. *J. Clin. Invest.* 125: 652–664. https://doi.org/10.1172/JCI77701

Gurnik, S., K. Devraj, J. Macas, M. Yamaji, J. Starke, A. Scholz, K. Sommer, M. Di Tacchio, R. Vutukuri, H. Beck, et al. 2016. Angiopoietin-2-induced blood-brain barrier compromise and increased stroke size are rescued by VE-PTP-dependent restoration of Tie2 signaling. *Acta Neuropathol.* 131:753–773. https://doi.org/10.1007/s00401-016-1551-3

Hart, M.J., X. Jiang, T. Kozasa, W. Roscoe, W.D. Singer, A.G. Gilman, P.C. Sternweis, and G. Bollag. 1998. Direct stimulation of the guanine nucleotide exchange activity of p115 RhoGEF by Galpha13. *Science.* 280: 2112–2114. https://doi.org/10.1126/science.280.5372.2112

Heupel, W.M., A. Efthymiadis, N. Schlegel, T. Müller, Y. Baumer, W. Baumgartner, D. Drenckhahn, and J. Waschke. 2009. Endothelial barrier stabilization by a cyclic tandem peptide targeting VE-cadherin transinteraction in vitro and in vivo. *J. Cell Sci.* 122:1616–1625. https://doi.org/10.1242/jcs.040212

Holinstat, M., D. Mehta, T. Kozasa, R.D. Minshall, and A.B. Malik. 2003. Protein kinase Calpha-induced p115RhoGEF phosphorylation signals endothelial cytoskeletal rearrangement. *J. Biol. Chem.* 278:28793–28798. https://doi.org/10.1074/jbc.M303900200

Hou, W.H., I.H. Liu, C.C. Tsai, F.E. Johnson, S.S. Huang, and J.S. Huang. 2011. CRSBP-1/LYVE-1 ligands disrupt lymphatic intercellular adhesion by inducing tyrosine phosphorylation and internalization of VE-cadherin. *J. Cell Sci.* 124:1231–1244. https://doi.org/10.1242/jcs.078154

Kofler, R., and G. Wick. 1977. Some methodologic aspects of the chromium chloride method for coupling antigen to erythrocytes. *J. Immunol. Methods.* 16:201–209. https://doi.org/10.1016/0022-1759(77)90198-3

Komarova, Y.A., F. Huang, M. Geyer, N. Daneshjou, A. Garcia, L. Idalino, B. Kreutz, D. Mehta, and A.B. Malik. 2012. VE-cadherin signaling induces EB3 phosphorylation to suppress microtubule growth and assemble adherens junctions. *Mol. Cell.* 48:914–925. https://doi.org/10.1016/j.molcel.2012.10.011

Komarova, Y.A., K. Kruse, D. Mehta, and A.B. Malik. 2017. Protein Interactions at Endothelial Junctions and Signaling Mechanisms Regulating Endothelial Permeability. *Circ. Res.* 120:179–206. https://doi.org/10.1161/CIRCRESAHA.116.306534

Kozasa, T., X. Jiang, M.J. Hart, P.M. Sternweis, W.D. Singer, A.G. Gilman, G. Bollag, and P.C. Sternweis. 1998. p115 RhoGEF, a GTPase activating protein for Galpha12 and Galpha13. *Science.* 280:2109–2111. https://doi.org/10.1126/science.280.5372.2109

Krendel, M., F.T. Zenke, and G.M. Bokoch. 2002. Nucleotide exchange factor GEF-H1 mediates cross-talk between microtubules and the actin cytoskeleton. *Nat. Cell Biol.* 4:294–301. https://doi.org/10.1038/ncb773

Kruse, K., Q.S. Lee, Y. Sun, J. Klomp, X. Yang, F. Huang, M.Y. Sun, S. Zhao, Z. Hong, S.M. Vogel, et al. 2019. N-cadherin signaling via Trio assembles adherens junctions to restrict endothelial permeability. *J. Cell Biol.* 218: 299–316. https://doi.org/10.1083/jcb.201802076

Lampugnani, M.G., M. Corada, L. Caveda, F. Breviario, O. Ayalon, B. Geiger, and E. Dejana. 1995. The molecular organization of endothelial cell to cell junctions: differential association of plakoglobin, beta-catenin, and alpha-catenin with vascular endothelial cadherin (VE-cadherin). *J. Cell Biol.* 129:203–217. https://doi.org/10.1083/jcb.129.1.203

Lampugnani, M.G., M. Corada, P. Andriopoulou, S. Esser, W. Risau, and E. Dejana. 1997. Cell confluence regulates tyrosine phosphorylation of adherens junction components in endothelial cells. *J. Cell Sci.* 110:2065–2077.

Lansbergen, G., Y. Komarova, M. Modesti, C. Wyman, C.C. Hoogenraad, H.V. Goodson, R.P. Lemaitre, D.N. Drechsel, E. van Munster, T.W. Gadella Jr., et al. 2004. Conformational changes in CLIP-170 regulate its binding to microtubules and dynactin localization. *J. Cell Biol.* 166:1003–1014. https://doi.org/10.1083/jcb.200402082

Lee, W.L., and A.S. Slutsky. 2010. Sepsis and endothelial permeability. *N. Engl. J. Med.* 363:689–691. https://doi.org/10.1056/NEJMcibr1007320

MacNevin, C.J., A. Toutchkine, D.J. Marston, C.W. Hsu, D. Tsygankov, L. Li, B. Liu, T. Qi, D.V. Nguyen, and K.M. Hahn. 2016. Ratiometric Imaging Using a Single Dye Enables Simultaneous Visualization of Rac1 and Cdc42 Activation. *J. Am. Chem. Soc.* 138:2571–2575. https://doi.org/10.1021/jacs.5b09764

Mamdouh, Z., A. Mikhailov, and W.A. Muller. 2009. Transcellular migration of leukocytes is mediated by the endothelial lateral border recycling compartment. *J. Exp. Med.* 206:2795–2808. https://doi.org/10.1084/jem.20082745

Nalbant, P., Y.C. Chang, J. Birkenfeld, Z.F. Chang, and G.M. Bokoch. 2009. Guanine nucleotide exchange factor-H1 regulates cell migration via localized activation of RhoA at the leading edge. *Mol. Biol. Cell.* 20: 4070–4082. https://doi.org/10.1091/mbc.e09-01-0041

Navarro, P., L. Caveda, F. Breviario, I. Mândoteanu, M.G. Lampugnani, and E. Dejana. 1995. Catenin-dependent and -independent functions of vascular endothelial cadherin. *J. Biol. Chem.* 270:30965–30972. https://doi.org/10.1074/jbc.270.52.30965

Nawroth, R., G. Poell, A. Ranft, S. Kloep, U. Samulowitz, G. Fachinger, M. Golding, D.T. Shima, U. Deutsch, and D. Vestweber. 2002. VE-PTP and VE-cadherin ectodomains interact to facilitate regulation of phosphorylation and cell contacts. *EMBO J.* 21:4885–4895. https://doi.org/10.1093/emboj/cdf497

Niu, J., J. Profirovic, H. Pan, R. Vaiskunaite, and T. Voyno-Yasenetskaya. 2003. G Protein betagamma subunits stimulate p114RhoGEF, a guanine nucleotide exchange factor for RhoA and Rac1: regulation of cell shape and reactive oxygen species production. *Circ. Res.* 93:848–856. https://doi.org/10.1161/01.RES.0000097607.14733.0C

Nottebaum, A.F., G. Cagna, M. Winderlich, A.C. Gamp, R. Linnepe, C. Polaschegg, K. Filippova, R. Lyck, B. Engelhardt, O. Kamenyeva, et al. 2008. VE-PTP maintains the endothelial barrier via plakoglobin and becomes dissociated from VE-cadherin by leukocytes and by VEGF. *J. Exp. Med.* 205:2929–2945. https://doi.org/10.1084/jem.20080406

Orsenigo, F., C. Giampietro, A. Ferrari, M. Corada, A. Galaup, S. Sigismund, G. Ristagno, L. Maddaluno, G.Y. Koh, D. Franco, et al. 2012. Phosphorylation of VE-cadherin is modulated by haemodynamic forces and contributes to the regulation of vascular permeability in vivo. *Nat. Commun.* 3:1208. https://doi.org/10.1038/ncomms2199

Pappenheimer, J.R., E.M. Renkin, and L.M. Borrero. 1951. Filtration, diffusion and molecular sieving through peripheral capillary membranes; a contribution to the pore theory of capillary permeability. *Am. J. Physiol.* 167:13–46. https://doi.org/10.1152/ajplegacy.1951.167.1.13

Pathak, R., V.D. Delorme-Walker, M.C. Howell, A.N. Anselmo, M.A. White, G. M. Bokoch, and C. Dermardirossian. 2012. The microtubule-associated Rho activating factor GEF-H1 interacts with exocyst complex to regulate vesicle traffic. *Dev. Cell.* 23:397–411. https://doi.org/10.1016/j.devcel.2012.06.014

Pertz, O., L. Hodgson, R.L. Klemke, and K.M. Hahn. 2006. Spatiotemporal dynamics of RhoA activity in migrating cells. *Nature.* 440:1069–1072. https://doi.org/10.1038/nature04665

Potter, M.D., S. Barbero, and D.A. Cheresh. 2005. Tyrosine phosphorylation of VE-cadherin prevents binding of p120- and beta-catenin and maintains the cellular mesenchymal state. *J. Biol. Chem.* 280:31906–31912. https://doi.org/10.1074/jbc.M505568200

Quaggin, S. 2017. VE-PTP knockout. IPO patent application WO/2017/190222. Mannin Research Inc., assignee. Issued November 9, 2017.

Ren, Y., R. Li, Y. Zheng, and H. Busch. 1998. Cloning and characterization of GEF-H1, a microtubule-associated guanine nucleotide exchange factor for Rac and Rho GTPases. *J. Biol. Chem.* 273:34954–34960. https://doi.org/10.1074/jbc.273.52.34954

Schossleitner, K., S. Rauscher, M. Gröger, H.P. Friedl, R. Finsterwalder, A. Habertheuer, M. Sibilia, C. Brostjan, D. Födinger, S. Citi, and P. Petzelbauer. 2016. Evidence That Cingulin Regulates Endothelial Barrier Function In Vitro and In Vivo. *Arterioscler. Thromb. Vasc. Biol.* 36: 647–654. https://doi.org/10.1161/ATVBAHA.115.307032

Schulte, D., V. Küppers, N. Dartsch, A. Broermann, H. Li, A. Zarbock, O. Kamenyeva, F. Kiefer, A. Khandoga, S. Massberg, and D. Vestweber. 2011. Stabilizing the VE-cadherin-catenin complex blocks leukocyte extravasation and vascular permeability. *EMBO J.* 30:4157–4170. https://doi.org/10.1038/emboj.2011.304

Shaw, S.K., P.S. Bamba, B.N. Perkins, and F.W. Luscinskas. 2001. Real-time imaging of vascular endothelial-cadherin during leukocyte transmigration across endothelium. *J. Immunol.* 167:2323–2330. https://doi.org/10.4049/jimmunol.167.4.2323

Shcherbakova, D.M., N. Cox Cammer, T.M. Huisman, V.V. Verkhusha, and L. Hodgson. 2018. Direct multiplex imaging and optogenetics of Rho GTPases enabled by near-infrared FRET. *Nat. Chem. Biol.* 14:591–600. https://doi.org/10.1038/s41589-018-0044-1

Shen, J., M. Frye, B.L. Lee, J.L. Reinardy, J.M. McClung, K. Ding, M. Kojima, H. Xia, C. Seidel, R. Lima e Silva, et al. 2014. Targeting VE-PTP activates TIE2 and stabilizes the ocular vasculature. *J. Clin. Invest.* 124:4564–4576. https://doi.org/10.1172/JCI74527

Siflinger-Birnboim, A., P.J. Del Vecchio, J.A. Cooper, F.A. Blumenstock, J.M. Shepard, and A.B. Malik. 1987. Molecular sieving characteristics of the cultured endothelial monolayer. *J. Cell. Physiol.* 132:111–117. https://doi.org/10.1002/jcp.1041320115

Souma, T., B.R. Thomson, S. Heinen, I.A. Carota, S. Yamaguchi, T. Onay, P. Liu, A.K. Ghosh, C. Li, V. Eremina, et al. 2018. Context-dependent functions of angiopoietin 2 are determined by the endothelial phosphatase VEPTP. *Proc. Natl. Acad. Sci. USA.* 115:1298–1303. https://doi.org/10.1073/pnas.1714446115

Tabdili, H., A.K. Barry, M.D. Langer, Y.H. Chien, Q. Shi, K.J. Lee, S. Lu, and D. E. Leckband. 2012. Cadherin point mutations alter cell sorting and modulate GTPase signaling. *J. Cell Sci.* 125:3299–3309. https://doi.org/10.1242/jcs.087395

Takeichi, M., and S. Nakagawa. 2001. Cadherin-dependent cell-cell adhesion. *Curr. Protoc. Cell Biol.* Chapter 9:Unit 9.3.

Tornavaca, O., M. Chia, N. Dufton, L.O. Almagro, D.E. Conway, A.M. Randi, M.A. Schwartz, K. Matter, and M.S. Balda. 2015. ZO-1 controls endothelial adherens junctions, cell-cell tension, angiogenesis, and barrier formation. *J. Cell Biol.* 208:821–838. https://doi.org/10.1083/jcb.201404140

Tsai, C.F., Y.T. Wang, Y.R. Chen, C.Y. Lai, P.Y. Lin, K.T. Pan, J.Y. Chen, K.H. Khoo, and Y.J. Chen. 2008. Immobilized metal affinity chromatography revisited: pH/acid control toward high selectivity in phosphoproteomics. *J. Proteome Res.* 7:4058–4069. https://doi.org/10.1021/pr800364d

Tse, J.R., and A.J. Engler. 2010. Preparation of hydrogel substrates with tunable mechanical properties. *Curr. Protoc. Cell Biol.* Chapter 10:Unit 10.16.

Vandenbroucke St Amant, E., M. Tauseef, S.M. Vogel, X.P. Gao, D. Mehta, Y. A. Komarova, and A.B. Malik. 2012. PKCα activation of p120-catenin serine 879 phospho-switch disassembles VE-cadherin junctions and disrupts vascular integrity. *Circ. Res.* 111:739–749. https://doi.org/10.1161/CIRCRESAHA.112.269654

van Nieuw Amerongen, G.P., S. van Delft, M.A. Vermeer, J.G. Collard, and V. W. van Hinsbergh. 2000. Activation of RhoA by thrombin in endothelial hyperpermeability: role of Rho kinase and protein tyrosine kinases. *Circ. Res.* 87:335–340. https://doi.org/10.1161/01.RES.87.4.335

Vestweber, D. 2012. Relevance of endothelial junctions in leukocyte extravasation and vascular permeability. *Ann. N. Y. Acad. Sci.* 1257:184–192. https://doi.org/10.1111/j.1749-6632.2012.06558.x

Vockel, M., and D. Vestweber. 2013. How T cells trigger the dissociation of the endothelial receptor phosphatase VE-PTP from VE-cadherin. *Blood.* 122:2512–2522. https://doi.org/10.1182/blood-2013-04-499228

von Thun, A., C. Preisinger, O. Rath, J.P. Schwarz, C. Ward, N. Monsefi, J. Rodríguez, A. Garcia-Munoz, M. Birtwistle, W. Bienvenut, et al. 2013. Extracellular signal-regulated kinase regulates RhoA activation and tumor cell plasticity by inhibiting guanine exchange factor H1 activity. *Mol. Cell. Biol.* 33:4526–4537. https://doi.org/10.1128/MCB.00585-13

Vouret-Craviari, V., C. Bourcier, E. Boulter, and E. van Obberghen-Schilling. 2002. Distinct signals via Rho GTPases and Src drive shape changes by thrombin and sphingosine-1-phosphate in endothelial cells. *J. Cell Sci.* 115:2475–2484.

Wallez, Y., F. Cand, F. Cruzalegui, C. Wernstedt, S. Souchelnytskyi, I. Vilgrain, and P. Huber. 2007. Src kinase phosphorylates vascular endothelial-cadherin in response to vascular endothelial growth factor: identification of tyrosine 685 as the unique target site. *Oncogene.* 26:1067–1077. https://doi.org/10.1038/sj.onc.1209855

Wessel, F., M. Winderlich, M. Holm, M. Frye, R. Rivera-Galdos, M. Vockel, R. Linnepe, U. Ipe, A. Stadtmann, A. Zarbock, et al. 2014. Leukocyte extravasation and vascular permeability are each controlled in vivo by different tyrosine residues of VE-cadherin. *Nat. Immunol.* 15:223–230. https://doi.org/10.1038/ni.2824

Winderlich, M., L. Keller, G. Cagna, A. Broermann, O. Kamenyeva, F. Kiefer, U. Deutsch, A.F. Nottebaum, and D. Vestweber. 2009. VE-PTP controls blood vessel development by balancing Tie-2 activity. *J. Cell Biol.* 185:657–671. https://doi.org/10.1083/jcb.200811159

Wójciak-Stothard, B., S. Potempa, T. Eichholtz, and A.J. Ridley. 2001. Rho and Rac but not Cdc42 regulate endothelial cell permeability. *J. Cell Sci.* 114:1343–1355.

Xiao, K., D.F. Allison, M.D. Kottke, S. Summers, G.P. Sorescu, V. Faundez, and A.P. Kowalczyk. 2003. Mechanisms of VE-cadherin processing and degradation in microvascular endothelial cells. *J. Biol. Chem.* 278:19199–19208. https://doi.org/10.1074/jbc.M211746200

Xiao, K., J. Garner, K.M. Buckley, P.A. Vincent, C.M. Chiasson, E. Dejana, V. Faundez, and A.P. Kowalczyk. 2005. p120-Catenin regulates clathrin-dependent endocytosis of VE-cadherin. *Mol. Biol. Cell.* 16:5141–5151. https://doi.org/10.1091/mbc.e05-05-0440

Yamada, S., and W.J. Nelson. 2007. Localized zones of Rho and Rac activities drive initiation and expansion of epithelial cell-cell adhesion. *J. Cell Biol.* 178:517–527. https://doi.org/10.1083/jcb.200701058

Yang, M.T., J. Fu, Y.K. Wang, R.A. Desai, and C.S. Chen. 2011. Assaying stem cell mechanobiology on microfabricated elastomeric substrates with geometrically modulated rigidity. *Nat. Protoc.* 6:187–213. https://doi.org/10.1038/nprot.2010.189

Yeh, Y.T., R. Serrano, J. François, J.J. Chiu, Y.J. Li, J.C. Del Álamo, S. Chien, and J.C. Lasheras. 2018. Three-dimensional forces exerted by leukocytes and vascular endothelial cells dynamically facilitate diapedesis. *Proc. Natl. Acad. Sci. USA.* 115:133–138. https://doi.org/10.1073/pnas.1717489115

Yuan, S.Y., and R.R. Rigor. 2010. *Regulation of Endothelial Barrier Function.* Morgan & Claypool Life Sciences, San Rafael, CA.

Zenke, F.T., M. Krendel, C. DerMardirossian, C.C. King, B.P. Bohl, and G.M. Bokoch. 2004. p21-activated kinase 1 phosphorylates and regulates 14-3-3 binding to GEF-H1, a microtubule-localized Rho exchange factor. *J. Biol. Chem.* 279:18392–18400. https://doi.org/10.1074/jbc.M400084200

Zhao, Y., K.K. Ting, J. Li, V.C. Cogger, J. Chen, A. Johansson-Percival, S.F. Ngiow, J. Holst, G. Grau, S. Goel, et al. 2017. Targeting Vascular Endothelial-Cadherin in Tumor-Associated Blood Vessels Promotes T-cell-Mediated Immunotherapy. *Cancer Res.* 77:4434–4447. https://doi.org/10.1158/0008-5472.CAN-16-3129